IgM Natural Antibodies Bind HLA-E-Leader Peptide Complexes and Modulate NK Cell Cytotoxicity

Dapeng Li[1,#], Simon Brackenridge[4,#], Lucy C. Walters[4,#], Karl Harlos[5], Daniel Rozbesky[5,6], Derek W. Cain[1,2], Kevin Wiehe[1,2], Richard M. Scearce[1], Maggie Barr[1], Zekun Mu[1], Robert Parks[1], Max Quastel[4], Robert J. Edwards[1,2], S. Munir Alam[1,2], Kevin O. Saunders[1,4], Persephone Borrow[4], E. Yvonne Jones[5], Geraldine M. Gillespie[4,*], Andrew J. McMichael[4,*], Barton F. Haynes[1,3,*]

[1]Duke Human Vaccine Institute, Duke University School of Medicine, Durham, NC 27710, USA

[2]Department of Medicine, Duke University School of Medicine, Durham, NC 27710, USA

[3]Department of Immunology, Duke University School of Medicine, Durham, NC 27710, USA

[4]Nuffield Department of Clinical Medicine, University of Oxford, Oxford, OX3 7FZ, UK

[5]Division of Structural Biology, Wellcome Centre for Human Genetics, University of Oxford, Oxford, OX3 7BN, UK

[6]Department of Cell Biology, Charles University, Prague, 12800, Czech Republic

[#]Authors contributed equally

*Address correspondence to geraldine.gillespie@ndm.ox.ac.uk, andrew.mcmichael@ndm.ox.ac.uk and barton.haynes@duke.edu

ABSTRACT (147 words)

The non-classical class Ib molecule human leukocyte antigen E (HLA-E) has limited polymorphism and can bind HLA class Ia leader sequence peptides (VL9). HLA-E-VL9 complexes interact with the natural killer (NK) cell inhibitory receptor NKG2A/CD94 and regulate NK cell-mediated cytotoxicity. Here we report a murine HLA-E-VL9-specific IgM monoclonal antibody 3H4 that enhanced killing of HLA-E-VL9-expressing target cells by a NKG2A^{+} NK cell line, most likely due to steric clashes between 3H4 and CD94/NKG2A when docked on the HLA-E-VL9 surface as determined by a 1.8 Å co-complex crystal structure. Key 3H4-mediated contacts with HLA-E-VL9 were generated by germline-encoded CDR-H3 residues. Human IgM HLA-E-VL9 reactive antibodies could also be isolated from CD10^{-}/CD27^{-} naïve B cells; these antibodies also recognized microbiome-derived peptides presented by HLA-E. Thus, a subset of natural antibodies that recognize VL9-bound HLA-E exist as part of the normal Ig repertoire with capacity to regulate NK cell function.

34 **INTRODUCTION**

35 Natural killer (NK) cells play critical roles in immune surveillance by discriminating non-self
36 from self, and function as effector cells by killing non-self malignant or pathogen-infected cells
37 and producing inflammatory cytokines (Chiossone et al., 2018; Raulet, 2006; Yokoyama and
38 Kim, 2006). Specific recognition of non-self by NK cells relies on a series of activating and
39 inhibitory receptors, including the killer immunoglobulin-like receptor (KIR) family and the
40 NKG2/CD94 heterodimeric receptors (Andre et al., 2018; Chiossone et al., 2018). NK cell
41 inhibitory receptors ligate human lymphocyte antigen (HLA) or major histocompatibility complex
42 (MHC) class I molecules expressed on healthy cells as self. Conversely, cells lacking MHC
43 class I are recognized by NK cells as "missing-self" and are sensitive to NK cell-mediated killing
44 (Ljunggren and Karre, 1985, 1990). In humans, KIRs recognize classical human HLA class Ia
45 molecules (Colonna and Samaridis, 1995; Karlhofer et al., 1992; Pende et al., 2019), whereas
46 the inhibitory NKG2A/CD94 heterodimeric receptor interacts with the non-classical HLA class Ib
47 molecule HLA-E and is balanced by an activating receptor NKG2C/CD94 (Braud et al., 1997;
48 Braud et al., 1998; Brooks et al., 1997). While KIRs expression is heterogeneous,,
49 NKG2A/CD94 is expressed on ~40% of human NK cells (Andre et al., 1999; Mahapatra et al.,
50 2017; Pende et al., 2019). Similarly, unlike classical HLA class I molecules, HLA-E has limited
51 polymorphism with only two predominant expressed variants HLA-E*01:01 and HLA-E*01:03
52 that differ only in residue 107, which is outside the peptide-binding groove (Kraemer et al.,
53 2014). The NKG2A/CD94/HLA-E pathway is considered as an important immune checkpoint
54 target and has recently become a focus for NK cell-based immunotherapeutic strategies (Hu et
55 al., 2019; Kim et al., 2019; Souza-Fonseca-Guimaraes et al., 2019). A subset of CD8+ T cells
56 also express NKG2A/CD94, and inhibition of NKG2A/CD94 - HLA-E interaction similarly has
57 application in CD8+ T cell-based immunotherapy (Andre et al., 2018; van Montfoort et al.,
58 2018).

59 HLA-E engages with NKG2A/CD94 via a restricted subset of peptides VMAPRT(L/V)
60 (V/L/I/F)L (designated VL9) that derive from the leader sequence of HLA-A, -C, -G and a third of
61 HLA-B molecules (Braud et al., 1997; Braud et al., 1998; Lee et al., 1998a; Lee et al., 1998b).
62 HLA-E binds VL9 peptides, which stabilize HLA-E surface expression (Braud et al., 1997; Braud
63 et al., 1998) on healthy host cells in which HLA-Ia expression is not perturbed and initiate
64 recognition by NKG2A/CD94 or NKG2C/CD94 on NK cells. The binding affinity of HLA-E-VL9
65 peptide complexes for NKG2A/CD94 is greater than that for NKG2C/CD94, such that the
66 inhibitory signal dominates to suppress aberrant NK cell-mediated cytotoxicity as well as
67 cytokine production (Aldrich et al., 1994; Braud et al., 1998; Kaiser et al., 2008; Llano et al.,
68 1998; Rolle et al., 2018). In addition, HLA-E and its murine or rhesus macaque homologs, is
69 capable of binding to a range of other host peptides and pathogen-derived peptides, including
70 heat-shock protein 60 (Hsp60)-derived peptides (Michaelsson et al., 2002), Mycobacterium
71 tuberculosis (Mtb) peptides (Joosten et al., 2010; van Meijgaarden et al., 2015), and simian
72 immunodeficiency virus (SIV) Gag peptides (Hansen et al., 2016), though unusually with a lower
73 affinity than VL9 (Walters et al., 2020). However, only VL9 peptide-loaded HLA-E can engage
74 CD94/NKG2A and protect cells from NK cell cytotoxicity (Kraemer et al., 2015; Michaelsson et
75 al., 2002; Sensi et al., 2009). Hence, leader sequence VL9 peptides are essential not only for
76 stabilizing HLA-E surface expression but also for determining the role of HLA-E/NKG2A/CD94
77 pathway in regulating NK cell self-recognition. However, it remains unclear if interruption of this
78 pathway by specifically targeting HLA-E-peptide complexes can enhance NK cell activity.
79 Natural antibodies are immunoglobulins that are present prior to simulation by cognate
80 antigen, and provide the first line of defence against bacterial, fungal and viral infections
81 (Holodick et al., 2017). They also suppress autoimmune, inflammatory and allergic responses,
82 protect from atherosclerotic vascular injury, and mediate apoptotic cell clearance (New et al.,
83 2016). Natural antibodies are generally near germline in sequence, have repertoire skewing of

84 IgM, IgA or IgE isotype, and respond to antigens with T cell independence (Holodick et al.,
85 2017). However, specific roles in regulation of natural killer (NK) cell functions are unknown.
86 Here, we define a mechanism of natural antibody modulation of NK cell killing whereby a
87 murine IgM monoclonal antibody (mAb) 3H4 bound to HLA-E-VL9 on target cells and enhanced
88 NK cytotoxicity of a NKG2A+ NK cell line. X-ray crystallographic analysis of an HLA-E-VL9/3H4
89 antigen-binding fragment (Fab) co-complex indicated that due to steric clashes, 3H4 and
90 CD94/NKG2A cannot simultaneously bind to what are essentially overlapping recognition
91 surfaces on HLA-E-VL9. Key Ig V(D)J residues in the 3H4-HLA-E-VL9 binding interface were
92 germline-encoded. Similarly, human HLA-E-VL9-reactive, near-germline IgMs were isolated
93 from the naïve B cell repertoire that recognized microbiome VL9-like peptides presented by
94 HLA-E. Thus, a subset of natural IgM HLA-E-VL9 antibodies exist *in vivo* that have the potential
95 to regulate NK cell cytotoxicity.
96
97 **RESULTS**
98 **Isolation of an HLA-E-VL9-specific mAb 3H4 from immunized transgenic mice**
99 With the original intention of raising monoclonal antibodies to the HIV-1 Gag peptide
100 RMYSPTSIL (RL9HIV) (the HIV counterpart of RL9SIV, one of the MHC-E binding SIV Gag
101 peptides identified by Hansen et al., 2016), we immunized human HLA-B27/β2-microglobulin
102 (β2M) transgenic mice (Taurog et al., 1990) (***Figures S1A-B***) with 293T cells transfected with
103 surface-expressed single chain HLA-E-RL9HIV complexes (Yu et al., 2002) (***Figure 1A*** and
104 ***S1C-D***). We produced hybridomas, and culture supernatants were screened for binding on a
105 panel of 293T cells transfected with single chain HLA-E-RL9HIV peptide complexes, or with
106 single chain HLA-E-VL9 peptide complexes as a control. Unexpectedly, we isolated a subset of
107 antibodies that specifically reacted with HLA-E-VL9 peptide, the most potent of which was the
108 IgM mAb 3H4. Unlike the well-characterized pan-HLA-E mAb 3D12 (Marin et al., 2003), 3H4
109 reacted specifically with HLA-E-VL9 (VMAPRTLVL) and not with control, non-VL9 HLA-E-

110 peptide complexes (***Figure 1B***). Mab 3H4 also bound to VL9 peptide-pulsed HLA-class I
111 negative K562 cells transfected with HLA-E (Lampen et al., 2013) (***Figure 1C***). Moreover, 3H4
112 bound to soluble HLA-E refolded with synthetic VL9 peptide in both ELISA (***Figure 1D***) and
113 surface plasmon resonance (SPR) assays (***Figure 1E***).
114
115 **HLA-E-VL9-specific mAb 3H4 is a minimally mutated pentameric IgM**
116 Sequence analysis of 3H4 mAb revealed 1.04% heavy chain variable region (V_H) and
117 2.51% light chain viable region (V_L) mutations *(**Table S1**).* We isolated 3 additional mAbs from
118 another two immunization studies (see methods). All four HLA-E-VL9-specific mouse antibodies
119 isolated were minimally mutated IgM (mean VH and VL mutations, 1.21% and 2.87%,
120 respectively) (***Table S1***). Negative stain electron microscopy showed that 3H4 was
121 predominantly pentameric with a small proportion of hexamers (***Figures S2A-B***). In addition,
122 3H4 was not autoreactive in anti-nuclear antibody or clinical autoantibody tests (***Figures S3A-***
123 ***B***).
124
125 **3H4 IgM enhances NK cell cytotoxicity against HLA-E-VL9-expressing target cells**
126 Given the suppressive role of the HLA-E-VL9/NKG2A/CD94 pathway in NK cell function, we
127 tested whether the binding of mAb 3H4 to HLA-E-VL9 could block NKG2A/CD94 interaction with
128 HLA-E and thereby release NK cell function (***Figure 2A***). A NKG2A/CD94 expressing human
129 NK cell line, NK92 (***Figure S4***), exhibited increased cytotoxicity against HLA-E-VL9
130 overexpressing cells in the presence of 3H4 IgM compared to an isotype control IgM (***Figure***
131 ***2B***). Next, we engineered the 3H4 variable regions into a human IgG2σ backbone (Saunders,
132 2019) (***Figure S5***). The 3H4-human IgG retained binding specificity for HLA-E-VL9, but showed
133 no cytotoxicity enhancement of NK cells (***Figure 2C***). In addition, we tested a combination of
134 3H4 with the NKG2A specific antibody, Z199. While blocking NKG2A enhanced NK killing
135 against HLA-E-VL9 expressing cells (***Figure 2D***), no further elevated killing was observed when

136 combining 3H4 with Z199 (***Figure 2E***), suggesting that killing enhancement was maximal with
137 3H4 alone. These data demonstrated that HLA-E-VL9-specific mAb 3H4 could enhance the
138 killing capacity of NKG2A+ NK cells, and this immunoregulatory role of 3H4 was dependent on
139 its IgM pentameric form, probably due to higher avidity binding.
140
141 **3H4 IgM recognizes the α1/α2 domain of HLA-E and N-terminus of the VL9 peptide**
142 To map the epitope on the HLA-E-VL9 complex recognized by 3H4, we tested 3H4 binding
143 to VL9 peptide presented by HLA-E, the rhesus ortholog Mamu-E, as well as two HLA-E/Mamu-
144 E hybrids – one with HLA-E α1/Mamu-E α2 (Hα1/Mα2), the other with Mamu-E α1/HLA-E α2
145 (Mα1/Hα2). 3H4 did not bind to Mamu-E/VL9 nor Hα1/Mα2-VL9, and its staining of cells
146 expressing Mα1/Hα2-VL9 was weak (***Figure 3A***), suggesting that 3H4 recognition involves
147 interaction with both α1 and α2 domains of HLA-E, and the epitope on α2 might be partially
148 conserved between human and rhesus. Moreover, VL9 mutation indicated that position 1 (P1) of
149 the peptide is important for 3H4 binding (***Figure 3B***), with antibody recognition of VL9 peptide
150 P1 variants with alanine, cysteine, isoleucine, serine, threonine, weak binding to histidine and
151 proline, but not those with arginine, glutamate, glycine, lysine, methionine, asparagine,
152 tryptophan, tyrosine or phenylalanine (***Figures 3C and S6***). These data suggest that mAb 3H4
153 makes contacts with both the HLA-E α1/α2 domain and the amino-terminal end of the VL9
154 peptide.
155
156 **Co-complex crystal structure of a 3H4 Fab bound to HLA-E-VL9**
157 We obtained a co-complex crystal structure of the 3H4 Fab bound to VL9 peptide-loaded
158 HLA-E, which packed in the C2 space group and diffracted to 1.8 Å (***Table S2***). Although two
159 copies of the co-complex were present in the asymmetric unit, a single copy constitutes the
160 focus of further discussion here since root-mean-square deviation (RMSD) calculations from
161 Cα-atom pairwise alignment of the two copies indicated minimal repositioning of interfacing

162 residues at the HLA-E-3H4 binding site (***Table S3***). Additionally, pairwise alignment with the
163 previously published non-receptor-bound HLA-E coordinates (PDB: 1MHE) (O'Callaghan et al.,
164 1998) revealed minimal structural changes in HLA-E upon 3H4 engagement (***Table S3B***).
165 3H4 docked onto the N-terminal region of the HLA-E-peptide-binding groove making
166 contacts with both α-helices of the HLA-E heavy chain in addition to residues 1-4 of the VL9
167 peptide (***Figures 4A-B***). The 3H4-HLA-E interface was mainly mediated via electrostatic
168 interactions and was dominated by the 3H4 VH chain segment which created a total buried
169 surface area of 1109.4 $Å^2$ and formed ten hydrogen bonds (H-bonds) and three salt bridges with
170 HLA-E residues of the α1-helix and one H-bond with T163 of the HLA-E α2-helix. By contrast,
171 the smaller 3H4 VL chain-HLA-E interface buried 522.8 $Å^2$ and involved only three inter-
172 molecular H-bonds and three salt bridges (***Tables S3 and S4***). Superposition of the 3H4-HLA-
173 E-VL9 co-complex with a previously published HLA-E-bound CD94/NKG2A structure (Kaiser et
174 al., 2008; Petrie et al., 2008) revealed steric clashes between the VH and VL domains of 3H4
175 and the CD94 and NKG2A subdomains, respectively (***Figures 4C-D***). Moreover, seven HLA-E
176 heavy chain residues (positions 58, 59, 62, 63 on the α1 helix and 162, 163 and 167 on the α2
177 helix) are shared between the 3H4-HLA-E and CD94/NKG2A-HLA-E footprints (***Figures 4E-F***).
178 Such steric clashes and overlapping footprints suggest simultaneous docking of these two HLA-
179 E binding partners, 3H4 and NKG2A/CD94, would be disallowed.
180

181 **Germline-encoded residues are critical for 3H4 contact with both HLA-E and VL9 peptide**

182 Remarkably, all four of the 3H4-derived residues that interface with the VL9 peptide (Y97,
183 S100, S100A and Y100B, Kabat numbering) reside within the VH CDR3 D-junction and are
184 germline-encoded. This 3H4-VL9 interface is characterized by weak Van der Waals and
185 hydrophobic contacts, such as those mediated between Y100B (3H4) and V1 or P4 (VL9)
186 (***Figure 4G***). Further, the positioning of the Y100B (3H4) side chain directly above V1 (VL9) in
187 part explains the preference for small side chains at this position of the peptide and the dramatic

188 reductions in 3H4 binding to HLA-E bound to VL9 variants with larger residues such as H or F at
189 position 1 (***Figure 3C***). Distinctive shape complementarity is also observed at the 3H4-VL9
190 interface with the side chains of S100 and S100A (3H4) wrapping around the cyclic side chain
191 of P4 (VL9).

192 The germline-encoded VH CDR3 D-junction residues that form the 3H4-VL9 interface (Y97,
193 S100, S100A and Y100B), also mediate key contacts with the HLA-E heavy chain. The surface
194 loop (residues A93-V102) containing these germline-encoded residues sweeps across the HLA-
195 E-peptide-binding groove forming H-bonds with both the α1 and α2 helices; T163 of the HLA-E
196 α2 helix forms a H-bond with S100 (3H4), and R62 of the HLA-E α1-helix forms two H-bonds
197 with the Y100B (3H4) mainchain and an additional H-bond with the main chain of S100A (3H4)
198 (***Figure 4H***). Moreover, Y100B (3H4) is involved in multiple polar pi stacking interactions. Not
199 only is the Y100B side chain sandwiched between R62 and W167 of the HLA-E α1 and α2
200 helices, respectively, R62 (HLA-E α1) is also positioned between the aromatic rings of Y100B
201 and W100D of the VH CDR3 domain.

202 Key contacts outside the germline-encoded CDR3 D-junction region are also formed at the
203 3H4 VH-HLA-E or 3H4 VL-HLA-E interfaces. For 3H4 HC, the VH CDR2 region (residues I51-
204 T57) is positioned above the HLA-E α1-helix where a string of inter-molecular H-bonds are
205 formed involving G56 and N54 of the VH CDR2 in addition to D50, Q61 and K64 of the
206 framework VH chain region (***Figure 4H***). Critically, R65 of the HLA-E α1-helix forms four H-
207 bonds with the 3H4 VH and also mediates polar pi stacking interactions with W100D of the VH
208 CDR3 loop. For 3H4 LC, D92 and E93 of the VL CDR3 loop H-bond with K170 of the HLA-E α2-
209 helix and N30 of the VL CDR1 loop forms an H-bond with the α2-helix residue, E166, of HLA-E
210 (***Figure 4I***). It is noteworthy that the four key interfacing residues of the 3H4 VH CDR3 D-
211 junction (Y97, S100, S100A and Y100B) are germline-encoded (***Figures 4J***). Since these
212 residues interface with both the HLA-E heavy chain and VL9 peptide, the B cell receptor

213 germline component plays a central role in the recognition of VL9-bound HLA-E complexes by
214 3H4.
215
216 **Germline-encoding HLA-E-VL9-specific antibodies exist in healthy humans**
217 That HLA-E-VL9-specific antibodies were isolated from mice immunized with an unrelated
218 peptide antigen (RL9HIV) implied that antibody 3H4 might be derived from the natural B cell
219 pool rather than induced by immunization. Therefore, we assessed binding of HLA-E-VL9
220 fluorescent tetramers to B cells from naïve HLA-B27/β2M TG mice and B6 mice, and found that
221 HLA-E-VL9-binding B cells existed in unimmunized mice (***Figure S7***). Additionally, all HLA-E-
222 VL9-specific antibodies were minimally mutated IgM antibodies (***Table S1***). These findings
223 raised the hypothesis that HLA-E-VL9-specific antibodies were natural antibodies in mice.
224 We next questioned if similar antibodies were present in humans. Using HLA-E-VL9
225 tetramers as probes, we identified B cells expressing HLA-E-VL9-specific B cell receptors
226 (BCRs) in four male, cytomegalovirus (CMV) seronegative human donors (***Figures 5A and S8,***
227 ***Table S5***). We isolated 56 HLA-E-VL9-specific antibodies (***Figure 5B, Table S6***) that
228 specifically reacted with HLA-E-VL9 complexes (***Figures S9-S10***). By performing more in-depth
229 analysis of the binding profiles of four representative antibodies - CA123, CA133, CA143 and
230 CA147, we found that these antibodies exhibited distinct binding specificities to VL9 peptide
231 variants (***Figure 5C***) in addition to differential cross-reactivities with rhesus Mamu-E-VL9 or
232 mouse Qa-1-VL9 complexes (***Figure S11A-D***). These data suggested that BCRs with diverse
233 recognition patterns on the HLA-E-VL9 complex are present in uninfected humans.
234 In different donors, the percentages of HLA-E-VL9-specific B cells in pan-B cells ($CD3^-$
235 $CD235^-CD14^-CD16^-CD19^+$) was 0.0009%-0.0023% (mean of 0.0014%) (***Figure 5D***). HLA-E-
236 VL9-specific B cells were $IgD^+IgM^{+/-}$ B cells, in which four cell subsets were observed (***Figure***
237 ***5E***) – $CD10^-CD27^-CD38^{+/-}$ naïve B cells (71.4%), $CD10^+CD27^-CD38^{++}$ immature or newly
238 formed B cells (Giltiay et al., 2019) (10.7%), and $CD10^-CD27^+CD38^-$ non-class-switched

239 memory cells, demonstrating that BCRs specifically targeting HLA-E-VL9 peptide existed in the
240 naïve B cell repertoire of healthy humans.
241
242 **V_H/V_L gene usage of HLA-E-VL9-specific antibodies**
243 Natural antibodies demonstrate Ig repertoire skewing (Holodick et al., 2017; New et al.,
244 2016). To characterize the human antibody gene usage of HLA-E-VL9 antibodies, we analyzed
245 the paired heavy chain and light chain gene sequences of 56 human HLA-E-VL9 antibodies,
246 and found 1 multiple-member clone containing 6 antibodies in donor LP021 (Kepler et al., 2014)
247 (***Table S7***). Next, we compared the 51 HLA-E-VL9-specific B cell clones with a reference
248 human antibody repertoire (DeKosky et al., 2015). Over 45% of the heavy chain variable region
249 (V_H) genes were VH3-21 or VH3-11 in HLA-E-VL9 antibodies, whereas less than 7% of the
250 control B cells used these two genes (***Figure 6A*** *and* ***Table S6***). HLA-E-VL9 antibodies light
251 chain variable region (V_κ/V_λ) also preferentially utilized IGKV3-15, IGKV1-39 and IGKV3-11
252 genes compared to controls (***Figure 6B*** *and* ***Table S6***). No J chain gene usage preference was
253 observed (***Figure S12)***. Moreover, HLA-E-VL9 antibodies showed a trend to have shorter heavy
254 chain complementarity determining region 3 (CDR3) lengths than the reference antibodies
255 (***Figure 6C***), while no difference was observed for light chain CDR3 (***Figure 6D***). Given HLA-E-
256 VL9 antibodies were all IgMs primarily from naïve or immature B cells, we compared the
257 mutation frequencies of 51 clones with a reference human antibody repertoire containing both
258 naïve and antigen-experienced antibodies (DeKosky et al., 2016). Both heavy and light chain
259 variable region genes exhibited low somatic mutation rates that were similar to naïve B cell
260 controls (***Figures 6E-F***). Thus, human HLA-E-VL9-specific antibodies were IgM, minimally
261 mutated and displayed skewed usage of VH3-21 and VH3-11 VHs and IGKV3-15, IGKV1-39
262 and IGKV3-11 VLs.
263

264 **HLA-E-VL9-specific mAbs recognize microbiome-derived VL9-like peptides presented by**
265 **HLA-E**

266 We identified microbiome-derived VL9-like peptides from the NCBI microbiome database
267 predicted by NetMHC to have HLA-E binding capacity (Andreatta and Nielsen, 2016; Nielsen et
268 al., 2003) (***Table S7***). Eight peptides with the highest HLA-E binding scores were synthesized
269 as 9 amino acid peptides, incubated with K562-E cells, and tested for mAb 3H4 HLA-E-VL9-
270 specific antibody binding. Seven out of eight microbiome sequence-derived peptides showed
271 strong HLA-E binding as indicated by the ability to stabilize and upregulate HLA-E expression,
272 as read out by staining with HLA-E reactive antibody, 3D12 (***Figures 7 and S13A***). Notably,
273 peptides with sequences very closely related to VL9 (VMAPRTLLL), VMPPRALLL (from
274 *Escherichia coli MS 175-1*), VMAGRTLLL (from *Stenotrophomonas sp.*) and VMAPRTKLL (from
275 *Pseudomonas formosensis*) were detected on K562-E cells by the HLA-E-peptide-antibody
276 3H4. Human HLA-E-VL9 antibodies CA143 and CA147 also reacted with *Pseudomonas*
277 *formosensis*-derived peptide VMAPRTKLL bound to HLA-E (Lin et al., 2013) (***Figures 7 and***
278 ***S13B-C***). These data demonstrate that microbiome-derived peptides in complex with HLA-E are
279 capable of binding to HLA-E-VL9-specific antibodies and raise the hypothesis that microbiome
280 peptides may be one type of antigen capable of stimulating B cells with HLA-E-VL9 peptide
281 specificity *in vivo.*
282

283 **DISCUSSION**

284 In this study, we have isolated and characterized antibodies reactive with HLA-E-VL9
285 peptide complexes, and found these antibodies were derived from the naïve IgM B cell BCR
286 repertoire in mice as well as in non-immunized, HCMV seronegative male humans. While more
287 than 80% of the HLA-E-VL9 reactive B cells were immature or naïve, a few showed a memory
288 or plasmablast phenotype. However, somatic mutations were minimal and the affinity was low.
289 The lack of class switching in HLA-E-VL9-specific antibodies may reflect self-tolerance of CD4 T

290 cells and a lack of help for maturation of these antibodies. While the mouse antibodies were
291 selected in the setting of HLA-E-unrelated peptide immunizations, they were minimally mutated
292 IgM antibodies, as were most of the antibodies isolated from un-infected human males.
293 Structural analysis of the HLA-E-VL9:3H4 Fab co-complex revealed that the 3H4 heavy chain
294 made key contacts with HLA-E and the VL9 peptide using germline-encoded residues in the
295 CDR-H3 (D) region (***Figure 4J***). However, 3H4 is a mouse antibody reacting with human HLA-
296 E-VL9. The HLA-E equivalent in C57BL/6xSJL mice is Qa1b which presents the very similar
297 class Ia signal peptide 'Qdm' AMAPRTLLL. Whilst 3H4 recognizes that peptide bound to HLA-E,
298 it does not bind to that peptide in Qa1b (***Figure S6B***). However, HLA-E-VL9-specific antibodies
299 were identified in the naïve B cell pool of healthy humans, so the question arises as to whether
300 such B cells, or the antibodies they can produce, play an important immunoregulatory role in
301 humans. If so, this might provide the selective force to maintain these enriched V genes in the
302 germline. Indeed, we demonstrated proof of concept that the 3H4 IgM HLA-E-VL9 antibody
303 could enhance NK cytotoxicity of NKG2A+ NK cells.
304 Autoantibodies to HLA-Ia (Alberu et al., 2007; Morales-Buenrostro et al., 2008) and HLA-E
305 heavy chains (Ravindranath et al., 2010a; Ravindranath et al., 2010b) have been detected in
306 non-alloimmunized males, and contribute to allograft damage (Hickey et al., 2016; McKenna et
307 al., 2000). It has been suggested that the HLA-E antibodies in non-alloimmunized humans could
308 be elicited by autoantigens derived from viral, bacterial, or environmental agents cross-reactive
309 with HLAs, or soluble HLA-E heavy chains that become immunogenic without the β2M subunit
310 (Alberu et al., 2007; Hickey et al., 2016; Ravindranath et al., 2010a; Ravindranath et al., 2010b).
311 Viruses, bacteria and other microbes could be the stimuli of such innate-adaptive immune
312 interaction. The best known example is human cytomegalovirus (HCMV) that encodes the VL9
313 sequence VMAPRTLIL in the leader sequence of its UL40 gene. This peptide is processed in a
314 TAP independent manner and presented bound to HLA-E at the cell surface to inhibit NK cell
315 killing and evade innate immune responses (Tomasec et al., 2000). This has not been reported

316 to elicit antibody responses, but HLA-E-UL40 peptide-specific T cells have been described
317 when the limited polymorphism in the HLA A, B and C sequences mismatches that of the virus
318 to overcome self-tolerance (Sullivan et al., 2015). However, these subjects in this study were all
319 HCMV seronegative, ruling out the possibility that these antibodies were HCMV-induced.
320 Similarly, that they were male excluded pregnancy induced priming. A recent study found that
321 mouse gut microbial antigens shaped the BCR repertoire by contributing to BCR selection and
322 affinity maturation (Chen et al., 2020). Therefore, we tested several potential HLA-E binding
323 peptides, with sequence similarities to VL9, derived from the human microbiome. Three of our
324 HLA-E-VL9 antibodies recognized a subset of these HLA-E-presented microbiome-derived VL9-
325 like peptides. These data imply that human microbial peptides could also be presented by HLA-
326 E, interact with HLA-E-VL9-bound naïve BCRs, and trigger expansion of B cells that express
327 HLA-E-VL9-specific BCRs.

328 Harnessing NK cells to attack tumor cells has emerged as an attractive strategy for cancer
329 immunotherapies (Guillerey et al., 2016; Lowry and Zehring, 2017). One of the most promising
330 targets for therapeutic immune-modulation of NK cell functions is the NKG2A/CD94-HLA-E-VL9
331 interaction. Monalizumab, the first-in-class monoclonal antibody checkpoint inhibitor targeting
332 NKG2A, enhances anti-tumor immunity by activating cytotoxic activities of effector CD8+ T cells
333 and NK cells (Andre et al., 2018; Creelan and Antonia, 2019; van Hall et al., 2019). In our study,
334 co-complex structural analysis revealed steric clashes between a 3H4 Fab and the NK inhibitory
335 receptor NKG2A/CD94 when docked onto HLA-E-VL9, which explained the mechanism of 3H4
336 IgM enhancing NKG2A+ NK cell killing. Notably, 3H4 IgM enhanced the cytotoxicity of an
337 NKG2A+ human NK cell line NK92, that is a safe and established cell line for adoptive
338 immunotherapy in phase I clinical trials (Klingemann et al., 2016). Therefore, 3H4 which targets
339 HLA-E-VL9 could have potential as an alternative to NKG2A targeting antibodies such as
340 Monalizumab as a check point inhibitor for immunotherapy.

341 In summary, our study has demonstrated a novel specificity of IgM natural antibodies, that
342 of recognition of HLA-E-VL9 peptide complexes, which suggests a NK cell immunoregulatory
343 role. The isolation of antibody 3H4 suggested that mouse could be a repository for this and
344 other anti-HLA-E-peptide antibodies that warrant further development as therapeutic agents.
345 Finally, the methods used here provide a means to rapidly isolate mAbs to other HLA/peptide
346 complexes such as HLA-E-SIV/HIV peptides (Hansen et al., 2016; Walters et al., 2018),
347 mycobacterium tuberculosis peptides (Joosten et al., 2010; McMurtrey et al., 2017; van
348 Meijgaarden et al., 2015), or HLA class I-presented neoantigen peptides that are derived from
349 mutated tumor tissues (Chen et al., 2019; Garcia-Garijo et al., 2019).
350
351
352 **MATERIALS AND METHODS**
353 **Cell Lines**
354 K562-E cells (K562 cells stably expressing HLA-E) and K562-E/UL49.5 cells (with a TAP-
355 inhibitor UL49.5) are kindly provided by Dr. Thorbald van Hall from Leiden University (Lampen
356 et al., 2013). All the other cells used in this study are from ATCC. 293T cells (ATCC CRL-3216)
357 were maintained in Dulbecco's Modified Eagle's Medium (DMEM; Gibco, Catalog# 10564)
358 supplemented with 10% fetal bovine serum (FBS; Gibco, Catalog# 10099141) and 1%
359 penicillin/streptomycin (Gibco, Catalog# 10378016). K562 cells (ATCC CCL-243), K562-E cells
360 and K562-E/UL49.5 cells were cultured in Iscove's Modified Dulbecco's Medium (IMDM;
361 Hyclone, Catalog# SH30228.01) supplemented with 10% FBS. Jurkat, DU-4475 and U-937 cells
362 were cultured in RPMI-1640 medium (Gibco, Catalog# 72400) supplemented with 10% FBS.
363 SiHa cells were cultured in Minimum Essential Medium (MEM; Gibco, Catalog# 11095080)
364 supplemented with 10% FBS. The NK-92 human cell line (ATCC CRL-2407) was cultured in
365 Alpha Minimum Essential medium (α-MEM; Gibco, Catalog# 12561072) supplemented with
366 2 mM L-glutamine, 0.2 mM inositol, 0.1 mM 2-mercaptoethanol, 0.02 mM folic acid, 100 U/ml

367 recombinant IL-2 (Biolegend, Catalog# 589108), 12.5% horse serum (Gibco, Catalog#
368 16050122) and 12.5% FBS. All the cells were maintained at 37°C, 5% CO2 in humidified
369 incubators.
370
371 **Animals**
372 Transgenic mice carrying human β2-microglobulin (β2m) and HLA-B*27:05 genes were
373 obtained from Jackson lab (B6.Cg-Tg(B2M,HLA-B*27:05)56-3Trg/DcrJ; Stock# 003428).
374 Hemizygous mice were used in this experiment, as this strain is homozygous lethal. For
375 hemizygous mice genotyping, peripheral blood lymphocytes (PBLs) were isolated and stained
376 using mouse CD45 antibody (Biolegend, Catalog# 103122), human HLA class I antibody
377 (Biolegend, Catalog# 311406) and human β2m antibody (Biolegend, Catalog# 316312). All
378 animal experiments were conducted with approved protocols from the Duke University
379 Institutional Animal Care and Use Committee.
380
381 **Human Subjects**
382 Human leukapheresis frozen vials were collected by the External Quality Assurance
383 Program Oversight Laboratory (EQAPOL) (Sanchez et al., 2014a; Sanchez et al., 2014b).
384 Samples from four male donors were used in this study. ***Table S5*** shows the clinical
385 characteristics of the individuals studied. All experiments that related to human subjects was
386 carried out with the informed consent of trial participants and in compliance with Institutional
387 Review Board protocols approved by Duke University Medical Center.
388
389 **Peptide synthesis**
390 The VL9 peptide (VMAPRTVLL) was synthesized to >85% purity via Fmoc (9-
391 fluorenylmethoxy carbonyl) chemistry by Genscript USA and reconstituted to 200mM in DMSO.
392

393 **HLA-E-peptide protein refolding and purification**

394 β2-microglobulin, previously purified from inclusion bodies in a Urea-MES buffer, was added
395 to a refolding buffer to achieve a final concentration of 2μM. The refold buffer comprised 100
396 mM Tris pH8.0, 400mM L-arginine monohydrochloride, 2mM EDTA, 5mM reduced glutathione
397 and 0.5mM oxidized Glutathione and was prepared in MiliQ water. A 20μM concentration of VL9
398 peptide (VMAPRTVLL), previously reconstituted to 200mM in DMSO, was added to the
399 refolding buffer followed by HLA-E*0103 heavy chain, which was pulsed into the refold to a final
400 concentration of 1μM. Once the refold had incubated for 72hrs at 4 °C it was filtered through a
401 1.0μm cellular nitrate membrane and concentrated in the VivaFlow 50R and VivaSpin Turbo
402 Ultrafiltration centrifugal systems with 10kDa molecular weight cut-offs. The concentrated
403 samples were injected onto a Superdex S75 16/60 column and refolded protein eluted
404 according to size into phosphate buffered saline (PBS). Eluted protein complexes were
405 validated by non-reducing SDS-PAGE electrophoresis on NuPAGE 12% Bis-Tris protein gels
406 and further concentrated via VivaSpin Turbo Ultrafiltration centrifugal device to 1.1mg/mL.
407

408 **HLA-E-peptide biotinylation and tetramer generation**

409 HLA-E-peptide samples requiring biotinylation were subsequently buffered exchanged on
410 Sephadex G-25 PD10 columns (GE Healthcare, UK) into 10mM Tris buffer using commercially
411 available BirA enzyme (Avidity, USA) following the manufacturer's instructions. Following
412 overnight biotinylation, protein samples were subsequently purified into 20mM Tris pH8,100mM
413 NaCl buffer or PBS on a HiLoad 16/600 Superdex 75pg column using an AKTA size exclusion
414 fast protein liquid chromatography (FPLC) system. Correctly folded β2m-HLA-E*01:03-
415 peptide complexes were subsequently concentrated to 2mg/mL and snap frozen.

416 HLA-E*01:03 tetramers were generated via conjugation to various fluorescent labels
417 including Extravidin-PE (Sigma), Streptavidin-bound APC (Biolegend, San Diego) or BV421
418 (Biolegend, San Diego) at a Molar ratio of 4:1 as previously described (Braud et al., 1998).

419

420 **Immunization in HLA-B27/β2m Transgenic Mice**

421 HLA-B27/β2m transgenic mice (*n*=23) were intramuscularly (i.m.) immunized with pooled
422 HLA-E-RL9HIV complex (12.5 µg/animal) and HLA-E-RL9SIV complex (12.5 µg/animal)
423 adjuvanted with STR8S-C at weeks 0, 2, 4, 6, 12 and 16. MAb 3H4 was isolated from one of the
424 mice in this study. In another experiment, HLA-B27/β2m transgenic mice (*n* = 10) were i.p.
425 immunized with either HLA-E-RL9HIV SCT transfected 293T cells ($2x10^6$ cells/animal) or HLA-
426 E-RL9SIV SCT transfected 293T cells ($2x10^6$ cells/animal) at weeks 0, 2, 4, 6, 17 and 19. In the
427 third experiment, HLA-B27/β2m transgenic mice (*n*=10) were i.m. immunized with HLA-E-VL9
428 complex (25 µg/animal) adjuvanted with STR8S-C at Week 0, 2 and 4, following by
429 intraperitoneally (i.p.) immunization with HLA-E-VL9 SCT transfected 293T cells ($2x10^6$
430 cells/animal) at Week 14, 16 and 18. Serum titers were monitored by ELISA Mice with high
431 binding antibody titers were selected for the subsequent spleen cell fusion and B cell sorting
432 experiments.

433

434 **Hybridoma Cell Line Generation and Monoclonal Antibody Production**

435 Mice were boosted with the indicated priming antigen 3 days prior to fusion. Spleen cells
436 were harvested and fused with NS0 murine myeloma cells using PEG1500 to generate
437 hybridomas. After 2 weeks, supernatant of hybridoma clones were collected and screened by
438 flow cytometry-based high throughput screening (HTS). Specifically, we tested for antibodies
439 differentially binding 293T cells transiently transfected with plasmid DNA expressing single
440 chain peptide-HLA-E-ß2m trimers so that they expressed HLA-E-RL9HIV, HLA-E-RL9SIV or
441 HLA-E-VL9 at the cell surface. Hybridomas cells that secreted HLA-E-VL9 antibodies were
442 cloned by limiting dilution for at least 5 rounds until the phenotypes of all limiting dilution wells
443 are identical. IgG mAbs were purified by protein G affinity chromatography, while IgM mAbs
444 were purified by ammonium sulfate precipitation and by Superose 6 column size-exclusion

445 chromatography in AKTA Fast Protein Liquid Chromatography (FPLC) system. The VH and VL
446 sequences of mAbs were amplified from hybridoma cell RNA using primers reported previously
447 (Tian et al., 2016; von Boehmer et al., 2016).
448
449 **Cell Surface Staining and High-Throughput Screening (HTS)**
450 HLA-E SCT constructs encoding HLA-E-VL9, HLA-E-RL9HIV, or HLA-E-RL9SIV were
451 transfected into 293T cells using GeneJuice transfection reagent (Novagen, Catalog# 70967).
452 For epitope mapping experiment, a panel of HLA-E-VL9 SCT constructs with single amino acid
453 mutations were transfected into 293T cells using the same method. Cells were dissociated with
454 0.1% EDTA at 48 hours post-transfection and stained with a Fixable Near-IR Dead Cell Stain Kit
455 (Thermo Fisher, Catalog# L34976). After washing, primary antibodies (supernatant from
456 hybridoma cells, supernatant from transfected cells, or purified antibodies) were added and
457 incubated with cells for 1 hour at 4°C, following by staining with 1:1000 diluted secondary
458 antibodies for 30 mins at 4°C. For mouse primary antibodies, we used Alexa Fluor 555 (AF555)
459 conjugated goat anti-mouse IgG (H+L) (Thermo Fisher, Catalog# A32727) or Alexa Fluor 647
460 (AF647) conjugated goat anti-mouse IgG (H+L) (Thermo Fisher, Catalog# A32728) as
461 secondary antibodies; for human primary antibodies, we used AF555 conjugated goat anti-
462 human IgG (H+L) (Thermo Fisher, Catalog# A-21433) or AF647 conjugated goat anti-human
463 IgG (H+L) (Thermo Fisher, Catalog# A-21445) as secondary antibodies. Cells were then
464 washed 3 times and resuspended in fixation buffer (1% formaldehyde in PBS, pH7.4). Data
465 were acquired on a BD LSR II flow cytometer and analyzed using FlowJo version 10.
466
467 **3H4 Fab production**
468 A humanized version of the 3H4 antibody (3H4-huIgG1) was digested to produce Fab
469 fragments using the Pierce Fab Preparation kit (ThermoFisher SCIENTIFIC). 3H4 Fab-retrieved
470 sample was further purified by size exclusion on a Superdex S75 16/60 column and eluted into

471 PBS buffer. Following concentration to 1.1mg/mL and SDS-PAGE gel-based validation, 3H4
472 Fab purified material was incubated for 1 hours on ice with freshly purified HLA-E-VL9. The
473 combined 3H4:Fab-HLA-E-VL9 sample was concentrated to 7.5mg/mL prior to crystallographic
474 set-up.
475
476 **Crystallization screening**
477 Crystals were grown via sitting drop vapour-diffusion at 20 °C in a 200nL drop with a 1:1
478 protein to reservoir ratio (Walter et al., 2005). The 3H4 Fab-HLA-E(VL9) co-complex crystallized
479 in 20% PEG 8000, 0.1 M Na HEPES at pH 7, in the ProPlex sparse matrix screen. Crystals
480 were cryo-preserved in 25% glycerol and diffraction data were collected at the I03 beamline of
481 Diamond Light Source.
482
483 **Crystallographic analysis**
484 Diffraction data were merged and indexed in xia2 dials (Winter et al., 2018). Outer shell
485 reflections were excluded from further analysis to ensure the $CC_{1/2}$ value exceeded the
486 minimum threshold (>0.5) in each shell (Karplus and Diederichs, 2012). Sequential molecular
487 replacement was carried out in MolRep of the CCP4i suite using molecule one of the previously
488 published Mtb44-bound HLA-E structure with the peptide coordinates deleted (PDB ID: 6GH4)
489 and one molecule of the previously published anti-APP-tag Fab structure (PDB ID: 6HGU) as
490 phasing models (Vagin and Teplyakov, 2010; Winn et al., 2011). Rigid body and retrained
491 refinement were subsequently carried out by Phenix.refine (Afonine et al., 2012) in between
492 manual model building in Coot (Emsley et al., 2010). Model geometry was validated by
493 MolProbity (Chen et al., 2010) and structural interpretation was conducted using the PyMOL
494 Molecular Graphics System, version 2.0 (Schrödinger, LLC) in addition to the PDBePISA
495 (Krissinel and Henrick, 2007) and PDBeFOLD (Krissinel and Henrick, 2004) servers.
496

497 **Antigen-Specific Single B Cell Sorting**

498 HLA-E-VL9-specific human B cells were sorted in flow cytometry using a three-color sorting
499 technique. Briefly, the stabilized HLA-E-β2M-peptide complexes were made as tetramers and
500 conjugated with different fluorophores. Human pan-B cells, including naïve and memory B cells,
501 were isolated from PBMCs of healthy donors using human pan-B cell enrichment kit
502 (STEMCELL, Catalog# 19554). The isolated pan-B cells were then stained with IgM PerCp-
503 Cy5.5 (Clone# G20-127, BD Biosciences, Catalog# 561285), IgD FITC (Clone# IA6-2, BD
504 Biosciences, Catalog# 555778), CD3 PE-Cy5 (Clone# HIT3a, BD Biosciences, Catalog#
505 555341), CD235a PE-Cy5 (Clone# GA-R2, BD Biosciences, Catalog# 559944), CD10 PE-
506 CF594 (Clone# HI10A, BD Biosciences, Catalog# 562396), CD27 PE-Cy7 (Clone# O323,
507 eBioscience, Catalog# 25-0279), CD16 BV570 (Clone# 3G8, Biolegend, Catalog# 302035),
508 CD14 BV605 (Clone# M5E2, Biolegend, Catalog# 301834), CD38 APC-AF700 (Clone# LS198-
509 4-2, Beckman Coulter, Catalog# B23489), CD19 APC-Cy7 (Clone# LJ25C1, BD Biosciences,
510 Catalog# 561743) and tetramers at 2 μg/million cells (including BV421-conjugated HLA-E-VL9
511 tetramer, PE-conjugated HLA-E-VL9 tetramer, APC-conjugated HLA-E-RL9SIV tetramer and
512 APC-conjugated HLA-E-RL9HIV tetramer). The cells were then stained with a Fixable Aqua
513 Dead Cell Stain Kit (Invitrogen, Catalog# L34957). HLA-E-VL9-specific B cells were sorted in
514 BD FACSAria II flow cytometer (BD Biosciences) for viable $CD3^{neg}$/ $CD14^{neg}$ /$CD16^{neg}$
515 /$CD235a^{neg}$/$CD19^{pos}$ / HLA-E-$VL9^{double\text{-}pos}$/ HLA-E-$RL9HIV^{neg}$/HLA-E-$RL9SIV^{neg}$ subset as single
516 cells in 96-well plates.

517

518 **PCR Amplification of Human Antibody Genes**

519 The $V_HD_HJ_H$ and V_LJ_L genes were amplified by RT-PCR from the flow cytometry-sorted
520 single B cells using the methods as described previously (Liao et al., 2009; Wrammert et al.,
521 2008) with modification. Primer details were listed in Tables S2. The PCR-amplified genes were
522 then purified and sequenced with 10 μM forward and reverse primers. Sequences were

523 analyzed by using the human library in Clonalyst for the VDJ arrangements of the
524 immunoglobulin *IGHV*, *IGKV*, and *IGLV* sequences and mutation frequencies (Kepler et al.,
525 2014). Clonal relatedness of $V_HD_HJ_H$ and V_LJ_L sequences was determined as previously
526 described (Liao et al., 2013).
527
528 **Expression of $V_HD_HJ_H$ and V_LJ_L as Full-Length IgG Recombinant mAbs**
529 Transient transfection of recombinant mAbs was performed as previously described (Liao et
530 al., 2009). Briefly, purified PCR products were used for overlapping PCR to generate linear
531 human antibody expression cassettes. The expression cassettes were transfected into 293i
532 cells using ExpiFectamine (Thermo Fisher Scientific, Catalog# A14525). The supernatant
533 samples containing recombinant antibodies were used for cell surface staining and HTS assay
534 to measure the binding reactivities.
535 The selected human antibody genes were then synthesized and cloned (GenScript) in a
536 human IgG1 backbone with 4A mutations to enhance antibody-dependent cell-mediated
537 cytotoxicity (ADCC) or a human IgG2σ backbone with mutations that abolish ADCC (Saunders,
538 2019). Recombinant IgG mAbs were then produced in HEK293i suspension cells by transfection
539 with ExpiFectamine and purified using Protein A resin. The purified mAbs were run in SDS-
540 PAGE for Coomassie blue staining and western blot. Antibodies with aggregation were further
541 purified in AKTA FPLC system using a Superdex 200 size-exclusion column.
542
543 **Surface Plasmon Resonance (SPR)**
544 Surface plasmon resonance assays were performed on a BIAcore 3000 instrument, and
545 data analysis was performed with BIAevaluation 3.0 software as previously described (Liao et
546 al., 2006). Briefly, streptavidin was directly immobilized to CM5 sensor chips, then biotinylated
547 HLA-E-peptide complexes (HLA-E-VL9, HLA-E-RL9SIV, HLA-E-RL9HIV and mock control)
548 were bound to the immobilized streptavidin. Purified mAbs flowed over CM5 sensor chips at

549 concentrations of 100 μg/ml, and antibody binding was monitored in real-time at 25°C with a
550 continuous flow of PBS at 30 μl/min.
551
552 **ELISA**
553 Direct binding ELISAs were conducted in 384-well ELISA plates coated with 2 μg/ml of C-
554 trap-stabilized HLA-E-VL9, C-trap-stabilized HLA-E-RL9HIV or C-trap-stabilized HLA-E-RL9SIV
555 in 0.1 M sodium bicarbonate overnight at 4°C. Plates were washed with PBS + 0.05% Tween 20
556 and blocked with 3% BSA in PBS at room temperature for 1 h. MAb samples were incubated for
557 1 h in 3-fold serial dilutions starting at 100 μg/ml, followed by washing with PBS-0.05% Tween
558 20. HRP-conjugated goat anti-human IgG secondary Ab (SouthernBiotech, catalog# 2040-05)
559 was diluted to 1: 10,000 in 1% BSA in PBS-0.05% Tween 20 and incubated at room
560 temperature for 1 h. For sandwich ELISA, 384-well ELISA plates were coated with HLA-E-VL9
561 antibodies in a 3-fold dilution starting from 100 μg/mL in 0.1 M sodium bicarbonate overnight at
562 4°C. Plates were washed with PBS + 0.05% Tween 20 and blocked with 3% BSA in PBS at
563 room temperature for 1 h. C-trap-stabilized HLA-E-VL9, C-trap-stabilized HLA-E-RL9HIV, C-
564 trap-stabilized HLA-E-RL9SIV, or diluent control were then added at 2 μg/mL and incubated at
565 room temperature for 1 h. After washing, HRP-conjugated anti-human β2M antibody (Biolegend,
566 catalog# 280303) were added at 0.2 μg/mL and incubated at room temperature for 1 h. These
567 plates were washed for 4 times and developed with tetramethylbenzidine substrate (SureBlue
568 Reserve). The reaction was stopped with 1 M HCl, and optical density at 450 nm (OD_{450}) was
569 determined.
570
571 **Antibody Poly-Reactivity Assays**
572 All mAbs isolated from mice and human were tested for ELISA binding to nine autoantigens
573 - Sjogren's syndrome antigen A (SSA), Sjogren's syndrome antigen (SSB), Smith antigen (Sm),
574 ribonucleoprotein (RNP), scleroderma 70 (Scl-70), Jo-1 antigen, double-stranded DNA

575 (dsDNA), centromere B (Cent B), and histone as previously described (Han et al., 2017; Liao et
576 al., 2011). Indirect immunofluorescence assay of mAbs binding to HEp-2 cells (Inverness
577 Medical Professional Diagnostics, Princeton, NJ) was performed as previously described
578 (Haynes et al., 2005; Liao et al., 2011). MAbs 2F5 (Yang et al., 2013) and 17B (Moore and
579 Sodroski, 1996) were used as positive and negative controls, respectively. All antibodies were
580 screened in two independent experiments.
581
582 **Negative Stain Electron Microscopy of IgM antibodies**
583 FPLC purified IgM antibodies were diluted to 0.08 mg/ml in HEPES-buffered saline (pH 7.4)
584 + 5% glycerol, and stained with 2% uranyl formate. Images were obtained with a Philips EM420
585 electron microscope at 82,000 magnification and processed in Relion 3.0.
586
587 **Microbiome-derived Peptide Prediction**
588 VL9 peptide sequence was first searched by similarity in NCBI microbial protein BLAST.
589 The BLAST results were then analyzed for HLA-E binding epitope prediction using HLA class I
590 peptide binding algorithms NetMHC 4.0 (Andreatta and Nielsen, 2016; Nielsen et al., 2003).
591 Epitopes that have HLA-E binding prediction scores > 0.1, length = 9 aa, and are relative to
592 human microbiome were synthesized for validation experiments.
593
594 **Peptide-Pulsing in K562-E Cells**
595 K562-E cells and K562-E/UL49.5 cells were resuspended with fresh IMDM media with 10%
596 FBS at $2x10^6$ cells/ml. Peptides were added into cell suspension at a final concentration of 100
597 μM. The cell/peptide mixtures were incubated at 26°C with 5% CO_2 for 20-22 hours and were
598 transferred to 37°C for 2 hours with 5% CO_2 before use. In the following mAb staining
599 experiment, medium with 100 μM peptides was used to maintain peptide concentration.
600

601 **NK Cell Cytotoxicity Assay**

602 NK Cell Cytotoxicity was measured by ^{51}Cr release assay. Human NK-92 cells were used
603 as effector cells in our study. Transfected 293T cells were used as target cells. Target cells
604 were counted, washed, resuspended in R10 at 1×10^7 cell/ml, and labeled with $Na_2{}^{51}CrO_4$ at 250
605 μCi/ml for 2 hours at 37°C. After washing three times using R10, cells were mixed with effector
606 cells in a final effector to target (E:T) ratio of 60:1 and 6:1 in triplicate wells in a flexible 96 well
607 round bottom plates (PerkinElmer, Catalog# 1450-401). The plates were inserted in flexible 96-
608 well plate cassettes (PerkinElmer, Catalog# 1450-101), sealed and incubated at 37°C for 4
609 hours. After the incubation, cells were pelleted by centrifugation, and from the top of the well,
610 add 25 ul of supernatant to a rigid 96 well isoplates (PerkinElmer, Catalog#1450-514) containing
611 150 ul of Ultima Gold LSC Cocktail (Sigma, Catalog# L8286). The plates were inserted in rigid
612 96-well plate cassettes (PerkinElmer, Catalog# 1450-105), sealed and counted on Perkin Elmer
613 Microbeta Triux 1450 counter. ^{51}Cr labeled target cells without effector cells were set as a
614 spontaneous release control, and ^{51}Cr labeled target cells mixed with detergent (2% Triton X-
615 100) were used as a maximum release control. The percentages of specific lysis were
616 calculated with the formulation: The Percentages of Specific Lysis (^{51}Cr Release %) =
617 [(Experimental Release – Spontaneous Release)/ (Maximum Release – Spontaneous Release)]
618 x 100.

619

620 **Statistics Analysis**

621 Data were plotted using Prism GraphPad 8.0 or visualized using the ComplexHeatmap R
622 package. Significant analysis was performed using two-tailed Mann-Whitney tests or chi-square
623 test of independence to compare differences between groups with $p\text{-value} < 0.05$ considered
624 significant.

625

626

627 **ACKNOWLEDGMENTS**

628 We thank Dr. Thorbald van Hall from Leiden University for kindly providing the K562-E cells
629 and K562-E/UL49.5 cells. We thank Duke Human Vaccine Institute (DHVI) programs and
630 finance staff for project oversight and the contributions of technical staff at the DHVI, including
631 Jordan Cocchiaro, Kelly Soderberg, Ahmed Yousef Abuahmad, Yunfei Wang, Giovanna
632 Hernandez, Esther Lee, Paige Power, Aja Sanzone, Brenna Harrington, Andrew Foulger,
633 Amanda Newman, Cindy Bowman, Grace Stevens, Laura Sutherland, Margaret Deyton, Victoria
634 Gee-Lai, Tarra Von Holle, Thad Gurley, Madison Berry, Kara Anasti, Katayoun Mansouri, Erika
635 Dunford, and Dawn Jones Marshall. We thank the DHVI Flow Cytometry Core for technical
636 assistance. This study was funded by the Collaboratory of AIDS Researchers for Eradication
637 (CARE; UM1AI126619), the Center for HIV/AIDS Vaccine Immunology-Immunogen Discovery
638 (CHAVI-ID; UMI-AI100645) grant and the Consortium for HIV/AIDS Vaccine Development grant
639 (CHAVD; UM1AI144371) from NIH/NIAID/DAIDS, and the Bill and Melinda Gates Foundation
640 OPP1108533.

641

642 **AUTHOR CONTRIBUTIONS**

643 D.L. immunized the mice, generated the hybridomas, sorted B cells, cloned the antibodies
644 and analyzed data. S.B. made single-chain trimer constructs, performed epitope mapping
645 experiments and analyzed data. G.G, L.W. and M.Q. prepared the antigens and HLA-E
646 tetramers. L.W., G.G., D.R. and K.H performed structural experiments with oversight from
647 E.Y.J.. D.W.C. helped with flow cytometry sorting set-up. R.S., R.P. and M.B. performed
648 hybridoma experiments, ELISA assays and help with ^{51}Cr release assays. R.J.E. oversaw
649 negative stain EM. M.A. supervised and interpreted the SPR experiments. K.W. oversaw and
650 performed antibody gene sequence analysis. Z.M. and M.B. helped with antibody isolation.
651 K.O.S. oversaw antigen production. P.B. provided advice on NK cell assays and contributed to

652 study design and data interpretation. B.F.H., G.G. D.L. and A.J.M. conceived, designed,
653 coordinated the study. D.L. and B.F.H. wrote the manuscript which was reviewed by all authors.
654

655 **DECLARATION OF INTERESTS**

656 D.L., S.B., G.G., A.J.M. and B.F.H. have patents submitted on select aspects of the material
657 in this paper.
658

659 **REFERENCES**

660 Afonine, P.V., Grosse-Kunstleve, R.W., Echols, N., Headd, J.J., Moriarty, N.W., Mustyakimov, M.,
661 Terwilliger, T.C., Urzhumtsev, A., Zwart, P.H., and Adams, P.D. (2012). Towards automated
662 crystallographic structure refinement with phenix.refine. Acta Crystallogr D Biol Crystallogr *68*,
663 352-367.
664 Alberu, J., Morales-Buenrostro, L.E., de Leo, C., Vargas-Rojas, M.I., Marino-Vazquez, L.A., and
665 Crispin, J.C. (2007). A non-allogeneic stimulus triggers the production of de novo HLA antibodies
666 in healthy adults. Transpl Immunol *18*, 166-171.
667 Aldrich, C.J., DeCloux, A., Woods, A.S., Cotter, R.J., Soloski, M.J., and Forman, J. (1994).
668 Identification of a Tap-dependent leader peptide recognized by alloreactive T cells specific for a
669 class Ib antigen. Cell *79*, 649-658.
670 Andre, P., Brunet, C., Guia, S., Gallais, H., Sampol, J., Vivier, E., and Dignat-George, F. (1999).
671 Differential regulation of killer cell Ig-like receptors and CD94 lectin-like dimers on NK and T
672 lymphocytes from HIV-1-infected individuals. Eur J Immunol *29*, 1076-1085.
673 Andre, P., Denis, C., Soulas, C., Bourbon-Caillet, C., Lopez, J., Arnoux, T., Blery, M., Bonnafous,
674 C., Gauthier, L., Morel, A.*, et al.* (2018). Anti-NKG2A mAb Is a Checkpoint Inhibitor that Promotes
675 Anti-tumor Immunity by Unleashing Both T and NK Cells. Cell *175*, 1731-1743 e1713.
676 Andreatta, M., and Nielsen, M. (2016). Gapped sequence alignment using artificial neural
677 networks: application to the MHC class I system. Bioinformatics *32*, 511-517.
678 Braud, V., Jones, E.Y., and McMichael, A. (1997). The human major histocompatibility complex
679 class Ib molecule HLA-E binds signal sequence-derived peptides with primary anchor residues at
680 positions 2 and 9. Eur J Immunol *27*, 1164-1169.

681 Braud, V.M., Allan, D.S., O'Callaghan, C.A., Soderstrom, K., D'Andrea, A., Ogg, G.S., Lazetic, S.,
682 Young, N.T., Bell, J.I., Phillips, J.H.*, et al.* (1998). HLA-E binds to natural killer cell receptors
683 CD94/NKG2A, B and C. Nature *391*, 795-799.
684 Brooks, A.G., Posch, P.E., Scorzelli, C.J., Borrego, F., and Coligan, J.E. (1997). NKG2A
685 complexed with CD94 defines a novel inhibitory natural killer cell receptor. J Exp Med *185*, 795-
686 800.
687 Chen, F., Zou, Z., Du, J., Su, S., Shao, J., Meng, F., Yang, J., Xu, Q., Ding, N., Yang, Y.*, et al.*
688 (2019). Neoantigen identification strategies enable personalized immunotherapy in refractory
689 solid tumors. J Clin Invest *129*, 2056-2070.
690 Chen, H., Zhang, Y., Ye, A.Y., Du, Z., Xu, M., Lee, C.S., Hwang, J.K., Kyritsis, N., Ba, Z., Neuberg,
691 D.*, et al.* (2020). BCR selection and affinity maturation in Peyer's patch germinal centres. Nature
692 *582*, 421-425.
693 Chen, V.B., Arendall, W.B., 3rd, Headd, J.J., Keedy, D.A., Immormino, R.M., Kapral, G.J., Murray,
694 L.W., Richardson, J.S., and Richardson, D.C. (2010). MolProbity: all-atom structure validation for
695 macromolecular crystallography. Acta Crystallogr D Biol Crystallogr *66*, 12-21.
696 Chiossone, L., Dumas, P.Y., Vienne, M., and Vivier, E. (2018). Natural killer cells and other innate
697 lymphoid cells in cancer. Nat Rev Immunol *18*, 671-688.
698 Colonna, M., and Samaridis, J. (1995). Cloning of immunoglobulin-superfamily members
699 associated with HLA-C and HLA-B recognition by human natural killer cells. Science *268*, 405-
700 408.
701 Creelan, B.C., and Antonia, S.J. (2019). The NKG2A immune checkpoint - a new direction in
702 cancer immunotherapy. Nat Rev Clin Oncol *16*, 277-278.
703 DeKosky, B.J., Kojima, T., Rodin, A., Charab, W., Ippolito, G.C., Ellington, A.D., and Georgiou,
704 G. (2015). In-depth determination and analysis of the human paired heavy- and light-chain
705 antibody repertoire. Nat Med *21*, 86-91.
706 DeKosky, B.J., Lungu, O.I., Park, D., Johnson, E.L., Charab, W., Chrysostomou, C., Kuroda, D.,
707 Ellington, A.D., Ippolito, G.C., Gray, J.J.*, et al.* (2016). Large-scale sequence and structural
708 comparisons of human naive and antigen-experienced antibody repertoires. Proc Natl Acad Sci
709 U S A *113*, E2636-2645.
710 Emsley, P., Lohkamp, B., Scott, W.G., and Cowtan, K. (2010). Features and development of Coot.
711 Acta Crystallogr D Biol Crystallogr *66*, 486-501.
712 Garcia-Garijo, A., Fajardo, C.A., and Gros, A. (2019). Determinants for Neoantigen Identification.
713 Front Immunol *10*, 1392.

714 Giltiay, N.V., Giordano, D., and Clark, E.A. (2019). The Plasticity of Newly Formed B Cells. J
715 Immunol *203*, 3095-3104.
716 Guillerey, C., Huntington, N.D., and Smyth, M.J. (2016). Targeting natural killer cells in cancer
717 immunotherapy. Nat Immunol *17*, 1025-1036.
718 Han, Q., Williams, W.B., Saunders, K.O., Seaton, K.E., Wiehe, K.J., Vandergrift, N., Von Holle,
719 T.A., Trama, A.M., Parks, R.J., Luo, K.*, et al.* (2017). HIV DNA-Adenovirus Multiclade Envelope
720 Vaccine Induces gp41 Antibody Immunodominance in Rhesus Macaques. J Virol *91*.
721 Hansen, S.G., Wu, H.L., Burwitz, B.J., Hughes, C.M., Hammond, K.B., Ventura, A.B., Reed, J.S.,
722 Gilbride, R.M., Ainslie, E., Morrow, D.W.*, et al.* (2016). Broadly targeted CD8(+) T cell responses
723 restricted by major histocompatibility complex E. Science *351*, 714-720.
724 Haynes, B.F., Fleming, J., St Clair, E.W., Katinger, H., Stiegler, G., Kunert, R., Robinson, J.,
725 Scearce, R.M., Plonk, K., Staats, H.F.*, et al.* (2005). Cardiolipin polyspecific autoreactivity in two
726 broadly neutralizing HIV-1 antibodies. Science *308*, 1906-1908.
727 Hickey, M.J., Valenzuela, N.M., and Reed, E.F. (2016). Alloantibody Generation and Effector
728 Function Following Sensitization to Human Leukocyte Antigen. Front Immunol *7*, 30.
729 Holodick, N.E., Rodriguez-Zhurbenko, N., and Hernandez, A.M. (2017). Defining Natural
730 Antibodies. Front Immunol *8*, 872.
731 Hu, W., Wang, G., Huang, D., Sui, M., and Xu, Y. (2019). Cancer Immunotherapy Based on
732 Natural Killer Cells: Current Progress and New Opportunities. Front Immunol *10*, 1205.
733 Joosten, S.A., van Meijgaarden, K.E., van Weeren, P.C., Kazi, F., Geluk, A., Savage, N.D.,
734 Drijfhout, J.W., Flower, D.R., Hanekom, W.A., Klein, M.R.*, et al.* (2010). Mycobacterium
735 tuberculosis peptides presented by HLA-E molecules are targets for human CD8 T-cells with
736 cytotoxic as well as regulatory activity. PLoS Pathog *6*, e1000782.
737 Kaiser, B.K., Pizarro, J.C., Kerns, J., and Strong, R.K. (2008). Structural basis for NKG2A/CD94
738 recognition of HLA-E. Proc Natl Acad Sci U S A *105*, 6696-6701.
739 Karlhofer, F.M., Ribaudo, R.K., and Yokoyama, W.M. (1992). MHC class I alloantigen specificity
740 of Ly-49+ IL-2-activated natural killer cells. Nature *358*, 66-70.
741 Karplus, P.A., and Diederichs, K. (2012). Linking crystallographic model and data quality. Science
742 *336*, 1030-1033.
743 Kepler, T.B., Munshaw, S., Wiehe, K., Zhang, R., Yu, J.S., Woods, C.W., Denny, T.N., Tomaras,
744 G.D., Alam, S.M., Moody, M.A.*, et al.* (2014). Reconstructing a B-Cell Clonal Lineage. II. Mutation,
745 Selection, and Affinity Maturation. Front Immunol *5*, 170.
746 Kim, N., Lee, H.H., Lee, H.J., Choi, W.S., Lee, J., and Kim, H.S. (2019). Natural killer cells as a
747 promising therapeutic target for cancer immunotherapy. Arch Pharm Res *42*, 591-606.

748 Klingemann, H., Boissel, L., and Toneguzzo, F. (2016). Natural Killer Cells for Immunotherapy -
749 Advantages of the NK-92 Cell Line over Blood NK Cells. Front Immunol *7*, 91.
750 Kraemer, T., Blasczyk, R., and Bade-Doeding, C. (2014). HLA-E: a novel player for
751 histocompatibility. J Immunol Res *2014*, 352160.
752 Kraemer, T., Celik, A.A., Huyton, T., Kunze-Schumacher, H., Blasczyk, R., and Bade-Doding, C.
753 (2015). HLA-E: Presentation of a Broader Peptide Repertoire Impacts the Cellular Immune
754 Response-Implications on HSCT Outcome. Stem Cells Int *2015*, 346714.
755 Krissinel, E., and Henrick, K. (2004). Secondary-structure matching (SSM), a new tool for fast
756 protein structure alignment in three dimensions. Acta Crystallogr D Biol Crystallogr *60*, 2256-2268.
757 Krissinel, E., and Henrick, K. (2007). Inference of macromolecular assemblies from crystalline
758 state. J Mol Biol *372*, 774-797.
759 Lampen, M.H., Hassan, C., Sluijter, M., Geluk, A., Dijkman, K., Tjon, J.M., de Ru, A.H., van der
760 Burg, S.H., van Veelen, P.A., and van Hall, T. (2013). Alternative peptide repertoire of HLA-E
761 reveals a binding motif that is strikingly similar to HLA-A2. Mol Immunol *53*, 126-131.
762 Lee, N., Goodlett, D.R., Ishitani, A., Marquardt, H., and Geraghty, D.E. (1998a). HLA-E surface
763 expression depends on binding of TAP-dependent peptides derived from certain HLA class I
764 signal sequences. J Immunol *160*, 4951-4960.
765 Lee, N., Llano, M., Carretero, M., Ishitani, A., Navarro, F., Lopez-Botet, M., and Geraghty, D.E.
766 (1998b). HLA-E is a major ligand for the natural killer inhibitory receptor CD94/NKG2A. Proc Natl
767 Acad Sci U S A *95*, 5199-5204.
768 Liao, H.X., Chen, X., Munshaw, S., Zhang, R., Marshall, D.J., Vandergrift, N., Whitesides, J.F.,
769 Lu, X., Yu, J.S., Hwang, K.K.*, et al.* (2011). Initial antibodies binding to HIV-1 gp41 in acutely
770 infected subjects are polyreactive and highly mutated. J Exp Med *208*, 2237-2249.
771 Liao, H.X., Levesque, M.C., Nagel, A., Dixon, A., Zhang, R., Walter, E., Parks, R., Whitesides, J.,
772 Marshall, D.J., Hwang, K.K.*, et al.* (2009). High-throughput isolation of immunoglobulin genes
773 from single human B cells and expression as monoclonal antibodies. J Virol Methods *158*, 171-
774 179.
775 Liao, H.X., Lynch, R., Zhou, T., Gao, F., Alam, S.M., Boyd, S.D., Fire, A.Z., Roskin, K.M.,
776 Schramm, C.A., Zhang, Z.*, et al.* (2013). Co-evolution of a broadly neutralizing HIV-1 antibody
777 and founder virus. Nature *496*, 469-476.
778 Liao, H.X., Sutherland, L.L., Xia, S.M., Brock, M.E., Scearce, R.M., Vanleeuwen, S., Alam, S.M.,
779 McAdams, M., Weaver, E.A., Camacho, Z.*, et al.* (2006). A group M consensus envelope
780 glycoprotein induces antibodies that neutralize subsets of subtype B and C HIV-1 primary viruses.
781 Virology *353*, 268-282.

782 Lin, S.Y., Hameed, A., Liu, Y.C., Hsu, Y.H., Lai, W.A., and Young, C.C. (2013). Pseudomonas
783 formosensis sp. nov., a gamma-proteobacteria isolated from food-waste compost in Taiwan. Int
784 J Syst Evol Microbiol *63*, 3168-3174.
785 Ljunggren, H.G., and Karre, K. (1985). Host resistance directed selectively against H-2-deficient
786 lymphoma variants. Analysis of the mechanism. J Exp Med *162*, 1745-1759.
787 Ljunggren, H.G., and Karre, K. (1990). In search of the 'missing self': MHC molecules and NK cell
788 recognition. Immunol Today *11*, 237-244.
789 Llano, M., Lee, N., Navarro, F., Garcia, P., Albar, J.P., Geraghty, D.E., and Lopez-Botet, M. (1998).
790 HLA-E-bound peptides influence recognition by inhibitory and triggering CD94/NKG2 receptors:
791 preferential response to an HLA-G-derived nonamer. Eur J Immunol *28*, 2854-2863.
792 Lowry, L.E., and Zehring, W.A. (2017). Potentiation of Natural Killer Cells for Cancer
793 Immunotherapy: A Review of Literature. Front Immunol *8*, 1061.
794 Mahapatra, S., Mace, E.M., Minard, C.G., Forbes, L.R., Vargas-Hernandez, A., Duryea, T.K.,
795 Makedonas, G., Banerjee, P.P., Shearer, W.T., and Orange, J.S. (2017). High-resolution
796 phenotyping identifies NK cell subsets that distinguish healthy children from adults. PLoS One *12*,
797 e0181134.
798 Marin, R., Ruiz-Cabello, F., Pedrinaci, S., Mendez, R., Jimenez, P., Geraghty, D.E., and Garrido,
799 F. (2003). Analysis of HLA-E expression in human tumors. Immunogenetics *54*, 767-775.
800 McKenna, R.M., Takemoto, S.K., and Terasaki, P.I. (2000). Anti-HLA antibodies after solid organ
801 transplantation. Transplantation *69*, 319-326.
802 McMurtrey, C., Harriff, M.J., Swarbrick, G.M., Duncan, A., Cansler, M., Null, M., Bardet, W.,
803 Jackson, K.W., Lewinsohn, D.A., Hildebrand, W.*, et al.* (2017). T cell recognition of
804 Mycobacterium tuberculosis peptides presented by HLA-E derived from infected human cells.
805 PLoS One *12*, e0188288.
806 Michaelsson, J., Teixeira de Matos, C., Achour, A., Lanier, L.L., Karre, K., and Soderstrom, K.
807 (2002). A signal peptide derived from hsp60 binds HLA-E and interferes with CD94/NKG2A
808 recognition. J Exp Med *196*, 1403-1414.
809 Moore, J.P., and Sodroski, J. (1996). Antibody cross-competition analysis of the human
810 immunodeficiency virus type 1 gp120 exterior envelope glycoprotein. J Virol *70*, 1863-1872.
811 Morales-Buenrostro, L.E., Terasaki, P.I., Marino-Vazquez, L.A., Lee, J.H., El-Awar, N., and Alberu,
812 J. (2008). "Natural" human leukocyte antigen antibodies found in nonalloimmunized healthy males.
813 Transplantation *86*, 1111-1115.
814 New, J.S., King, R.G., and Kearney, J.F. (2016). Manipulation of the glycan-specific natural
815 antibody repertoire for immunotherapy. Immunol Rev *270*, 32-50.

816 Nielsen, M., Lundegaard, C., Worning, P., Lauemoller, S.L., Lamberth, K., Buus, S., Brunak, S.,
817 and Lund, O. (2003). Reliable prediction of T-cell epitopes using neural networks with novel
818 sequence representations. Protein Sci *12*, 1007-1017.
819 O'Callaghan, C.A., Tormo, J., Willcox, B.E., Braud, V.M., Jakobsen, B.K., Stuart, D.I., McMichael,
820 A.J., Bell, J.I., and Jones, E.Y. (1998). Structural features impose tight peptide binding specificity
821 in the nonclassical MHC molecule HLA-E. Mol Cell *1*, 531-541.
822 Pende, D., Falco, M., Vitale, M., Cantoni, C., Vitale, C., Munari, E., Bertaina, A., Moretta, F., Del
823 Zotto, G., Pietra, G.*, et al.* (2019). Killer Ig-Like Receptors (KIRs): Their Role in NK Cell Modulation
824 and Developments Leading to Their Clinical Exploitation. Front Immunol *10*, 1179.
825 Petrie, E.J., Clements, C.S., Lin, J., Sullivan, L.C., Johnson, D., Huyton, T., Heroux, A., Hoare,
826 H.L., Beddoe, T., Reid, H.H.*, et al.* (2008). CD94-NKG2A recognition of human leukocyte antigen
827 (HLA)-E bound to an HLA class I leader sequence. J Exp Med *205*, 725-735.
828 Raulet, D.H. (2006). Missing self recognition and self tolerance of natural killer (NK) cells. Semin
829 Immunol *18*, 145-150.
830 Ravindranath, M.H., Kaneku, H., El-Awar, N., Morales-Buenrostro, L.E., and Terasaki, P.I.
831 (2010a). Antibodies to HLA-E in nonalloimmunized males: pattern of HLA-Ia reactivity of anti-
832 HLA-E-positive sera. J Immunol *185*, 1935-1948.
833 Ravindranath, M.H., Taniguchi, M., Chen, C.W., Ozawa, M., Kaneku, H., El-Awar, N., Cai, J., and
834 Terasaki, P.I. (2010b). HLA-E monoclonal antibodies recognize shared peptide sequences on
835 classical HLA class Ia: relevance to human natural HLA antibodies. Mol Immunol *47*, 1121-1131.
836 Rolle, A., Meyer, M., Calderazzo, S., Jager, D., and Momburg, F. (2018). Distinct HLA-E Peptide
837 Complexes Modify Antibody-Driven Effector Functions of Adaptive NK Cells. Cell Rep *24*, 1967-
838 1976 e1964.
839 Sanchez, A.M., DeMarco, C.T., Hora, B., Keinonen, S., Chen, Y., Brinkley, C., Stone, M., Tobler,
840 L., Keating, S., Schito, M.*, et al.* (2014a). Development of a contemporary globally diverse HIV
841 viral panel by the EQAPOL program. J Immunol Methods *409*, 117-130.
842 Sanchez, A.M., Rountree, W., Berrong, M., Garcia, A., Schuetz, A., Cox, J., Frahm, N., Manak,
843 M., Sarzotti-Kelsoe, M., D'Souza, M.P.*, et al.* (2014b). The External Quality Assurance Oversight
844 Laboratory (EQAPOL) proficiency program for IFN-gamma enzyme-linked immunospot (IFN-
845 gamma ELISpot) assay. J Immunol Methods *409*, 31-43.
846 Saunders, K.O. (2019). Conceptual Approaches to Modulating Antibody Effector Functions and
847 Circulation Half-Life. Front Immunol *10*, 1296.
848 Sensi, M., Pietra, G., Molla, A., Nicolini, G., Vegetti, C., Bersani, I., Millo, E., Weiss, E., Moretta,
849 L., Mingari, M.C.*, et al.* (2009). Peptides with dual binding specificity for HLA-A2 and HLA-E are

850 encoded by alternatively spliced isoforms of the antioxidant enzyme peroxiredoxin 5. Int Immunol
851 *21*, 257-268.
852 Souza-Fonseca-Guimaraes, F., Cursons, J., and Huntington, N.D. (2019). The Emergence of
853 Natural Killer Cells as a Major Target in Cancer Immunotherapy. Trends Immunol *40*, 142-158.
854 Sullivan, L.C., Westall, G.P., Widjaja, J.M., Mifsud, N.A., Nguyen, T.H., Meehan, A.C., Kotsimbos,
855 T.C., and Brooks, A.G. (2015). The Presence of HLA-E-Restricted, CMV-Specific CD8+ T Cells
856 in the Blood of Lung Transplant Recipients Correlates with Chronic Allograft Rejection. PLoS One
857 *10*, e0135972.
858 Taurog, J., Hammer, R., Maika, S., Sams, K., El-Zaatari, F., Stimpson, S., and Schwab, J. (1990).
859 HLA-B27 transgenic mice as potential models of human disease. In Transgenic mice and mutants
860 in MHC research (Springer), pp. 268-275.
861 Tian, M., Cheng, C., Chen, X., Duan, H., Cheng, H.L., Dao, M., Sheng, Z., Kimble, M., Wang, L.,
862 Lin, S.*, et al.* (2016). Induction of HIV Neutralizing Antibody Lineages in Mice with Diverse
863 Precursor Repertoires. Cell *166*, 1471-1484 e1418.
864 Tomasec, P., Braud, V.M., Rickards, C., Powell, M.B., McSharry, B.P., Gadola, S., Cerundolo, V.,
865 Borysiewicz, L.K., McMichael, A.J., and Wilkinson, G.W. (2000). Surface expression of HLA-E,
866 an inhibitor of natural killer cells, enhanced by human cytomegalovirus gpUL40. Science *287*,
867 1031.
868 Vagin, A., and Teplyakov, A. (2010). Molecular replacement with MOLREP. Acta Crystallogr D
869 Biol Crystallogr *66*, 22-25.
870 van Hall, T., Andre, P., Horowitz, A., Ruan, D.F., Borst, L., Zerbib, R., Narni-Mancinelli, E., van
871 der Burg, S.H., and Vivier, E. (2019). Monalizumab: inhibiting the novel immune checkpoint
872 NKG2A. J Immunother Cancer *7*, 263.
873 van Meijgaarden, K.E., Haks, M.C., Caccamo, N., Dieli, F., Ottenhoff, T.H., and Joosten, S.A.
874 (2015). Human CD8+ T-cells recognizing peptides from Mycobacterium tuberculosis (Mtb)
875 presented by HLA-E have an unorthodox Th2-like, multifunctional, Mtb inhibitory phenotype and
876 represent a novel human T-cell subset. PLoS Pathog *11*, e1004671.
877 van Montfoort, N., Borst, L., Korrer, M.J., Sluijter, M., Marijt, K.A., Santegoets, S.J., van Ham, V.J.,
878 Ehsan, I., Charoentong, P., Andre, P.*, et al.* (2018). NKG2A Blockade Potentiates CD8 T Cell
879 Immunity Induced by Cancer Vaccines. Cell *175*, 1744-1755 e1715.
880 von Boehmer, L., Liu, C., Ackerman, S., Gitlin, A.D., Wang, Q., Gazumyan, A., and Nussenzweig,
881 M.C. (2016). Sequencing and cloning of antigen-specific antibodies from mouse memory B cells.
882 Nat Protoc *11*, 1908-1923.

883 Walter, T.S., Diprose, J.M., Mayo, C.J., Siebold, C., Pickford, M.G., Carter, L., Sutton, G.C.,
884 Berrow, N.S., Brown, J., Berry, I.M.*, et al.* (2005). A procedure for setting up high-throughput
885 nanolitre crystallization experiments. Crystallization workflow for initial screening, automated
886 storage, imaging and optimization. Acta Crystallogr D Biol Crystallogr *61*, 651-657.
887 Walters, L.C., Harlos, K., Brackenridge, S., Rozbesky, D., Barrett, J.R., Jain, V., Walter, T.S.,
888 O'Callaghan, C.A., Borrow, P., Toebes, M.*, et al.* (2018). Pathogen-derived HLA-E bound
889 epitopes reveal broad primary anchor pocket tolerability and conformationally malleable peptide
890 binding. Nat Commun *9*, 3137.
891 Walters, L.C., McMichael, A.J., and Gillespie, G.M. (2020). Detailed and atypical HLA-E peptide
892 binding motifs revealed by a novel peptide exchange binding assay. Eur J Immunol.
893 Winn, M.D., Ballard, C.C., Cowtan, K.D., Dodson, E.J., Emsley, P., Evans, P.R., Keegan, R.M.,
894 Krissinel, E.B., Leslie, A.G., McCoy, A.*, et al.* (2011). Overview of the CCP4 suite and current
895 developments. Acta Crystallogr D Biol Crystallogr *67*, 235-242.
896 Winter, G., Waterman, D.G., Parkhurst, J.M., Brewster, A.S., Gildea, R.J., Gerstel, M., Fuentes-
897 Montero, L., Vollmar, M., Michels-Clark, T., Young, I.D.*, et al.* (2018). DIALS: implementation and
898 evaluation of a new integration package. Acta Crystallogr D Struct Biol *74*, 85-97.
899 Wrammert, J., Smith, K., Miller, J., Langley, W.A., Kokko, K., Larsen, C., Zheng, N.Y., Mays, I.,
900 Garman, L., Helms, C.*, et al.* (2008). Rapid cloning of high-affinity human monoclonal antibodies
901 against influenza virus. Nature *453*, 667-671.
902 Yang, G., Holl, T.M., Liu, Y., Li, Y., Lu, X., Nicely, N.I., Kepler, T.B., Alam, S.M., Liao, H.X., Cain,
903 D.W.*, et al.* (2013). Identification of autoantigens recognized by the 2F5 and 4E10 broadly
904 neutralizing HIV-1 antibodies. J Exp Med *210*, 241-256.
905 Yokoyama, W.M., and Kim, S. (2006). How do natural killer cells find self to achieve tolerance?
906 Immunity *24*, 249-257.
907 Yu, Y.Y., Netuschil, N., Lybarger, L., Connolly, J.M., and Hansen, T.H. (2002). Cutting edge:
908 single-chain trimers of MHC class I molecules form stable structures that potently stimulate
909 antigen-specific T cells and B cells. J Immunol *168*, 3145-3149.
910

911

912 **FIGURES**

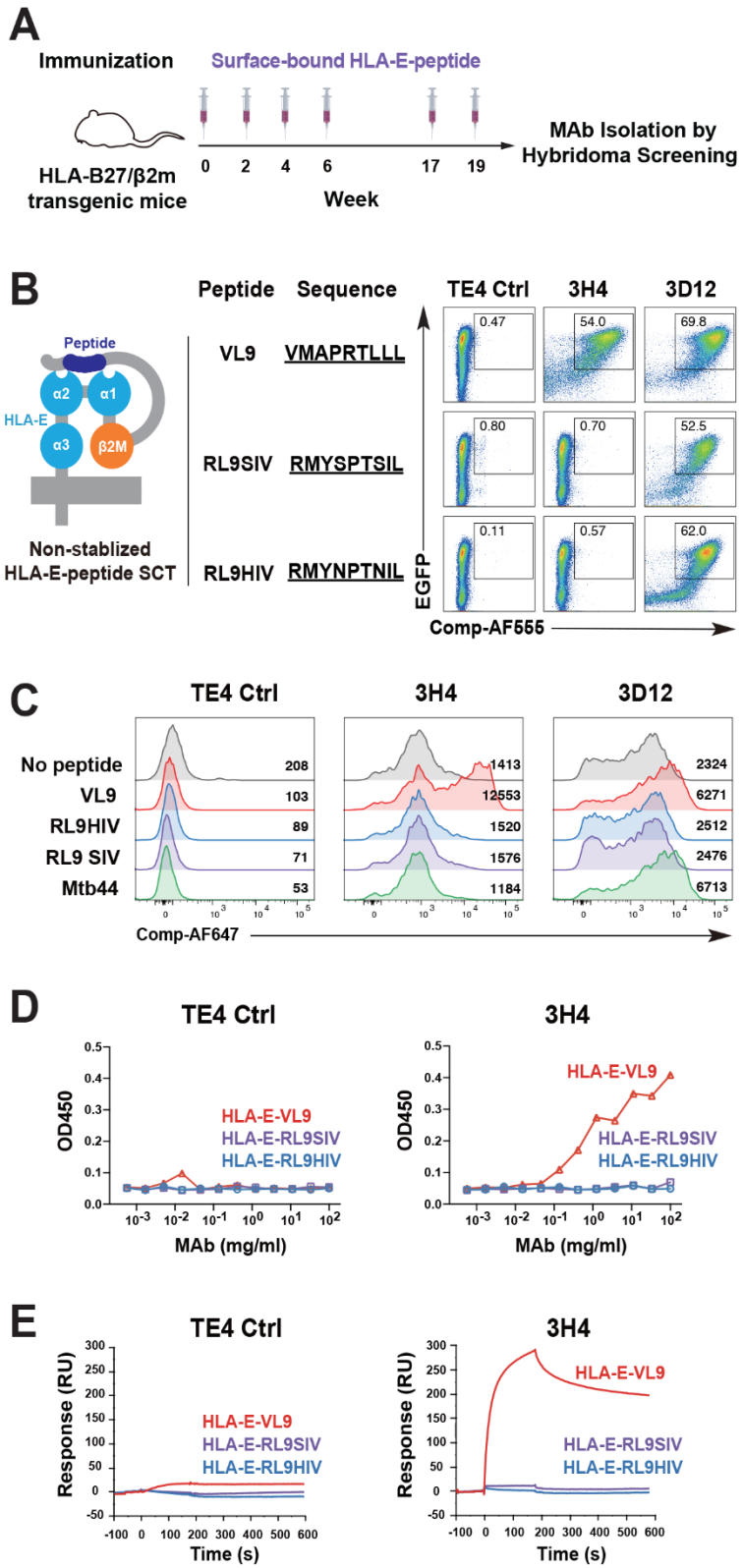

913

914 **Figure 1. Isolation of monoclonal antibodies specifically targeting HLA-E-VL9 complex.**
915 **(A) HLA-E specific antibodies elicited by vaccination.** HLA-B27/β2M transgenic (TG) mice
916 (*n*=10) were used to minimize the induction of antibodies to HLA class I and β2M. Animals were
917 immunized with cell surface-expressing HLA-E-RL9 peptide (a peptide derived from HIV-1;
918 denoted RL9HIV hereafter) single-chain trimer (SCT)-transfected 293T cells (indicated by red
919 arrows).
920 **(B) 3H4 bound HLA-E-VL9 SCT-transfected 293T cells.** All SCT constructs express EGFP to
921 indicate transfection efficiency. Transfected cells were stained with testing antibody and then an
922 Alexa fluor 555 (AF555)-anti-mouse Ig(H+L) secondary antibody. A control mouse IgM TE4 was
923 used as a negative control. Anti-pan-HLA-E antibody 3D12 was used as a positive control.
924 **(C) 3H4 bound VL9 peptide pulsed K562-HLA-E cells.** RL9HIV, RL9SIV, Mtb44 peptides
925 served as peptide controls. TE4 and 3D12 were used as antibody controls. Peptide-pulsed cells
926 were stained with testing antibody and then an Alexa fluor 647 (AF647)-anti-mouse Ig(H+L)
927 secondary antibody. Mean fluorescence intensity (MFI) of each sample is shown.
928 **(D-E) 3H4 specifically bound to soluble HLA-E-VL9 complexes as measured by ELISA**
929 **and SPR**. (D) ELISA plates were coated with 3H4 or control IgM TE4 in serial dilution, blocked,
930 and incubated with C-trap-stabilized HLA-E-VL9, HLA-E-RL9HIV, HLA-E-RL9SIV antigens.
931 After washing, antigen binding was detected by adding HRP-conjugated anti-human β2M
932 antibody. (E) For SPR, biotinylated HLA-E-peptide complexes (HLA-E-VL9, HLA-E-RL9SIV,
933 HLA-E-RL9HIV and mock control) were bound to the immobilized streptavidin. Antibody 3H4
934 and control TE4 were flowed over sensor chips and antibody binding was monitored in real-
935 time.
936

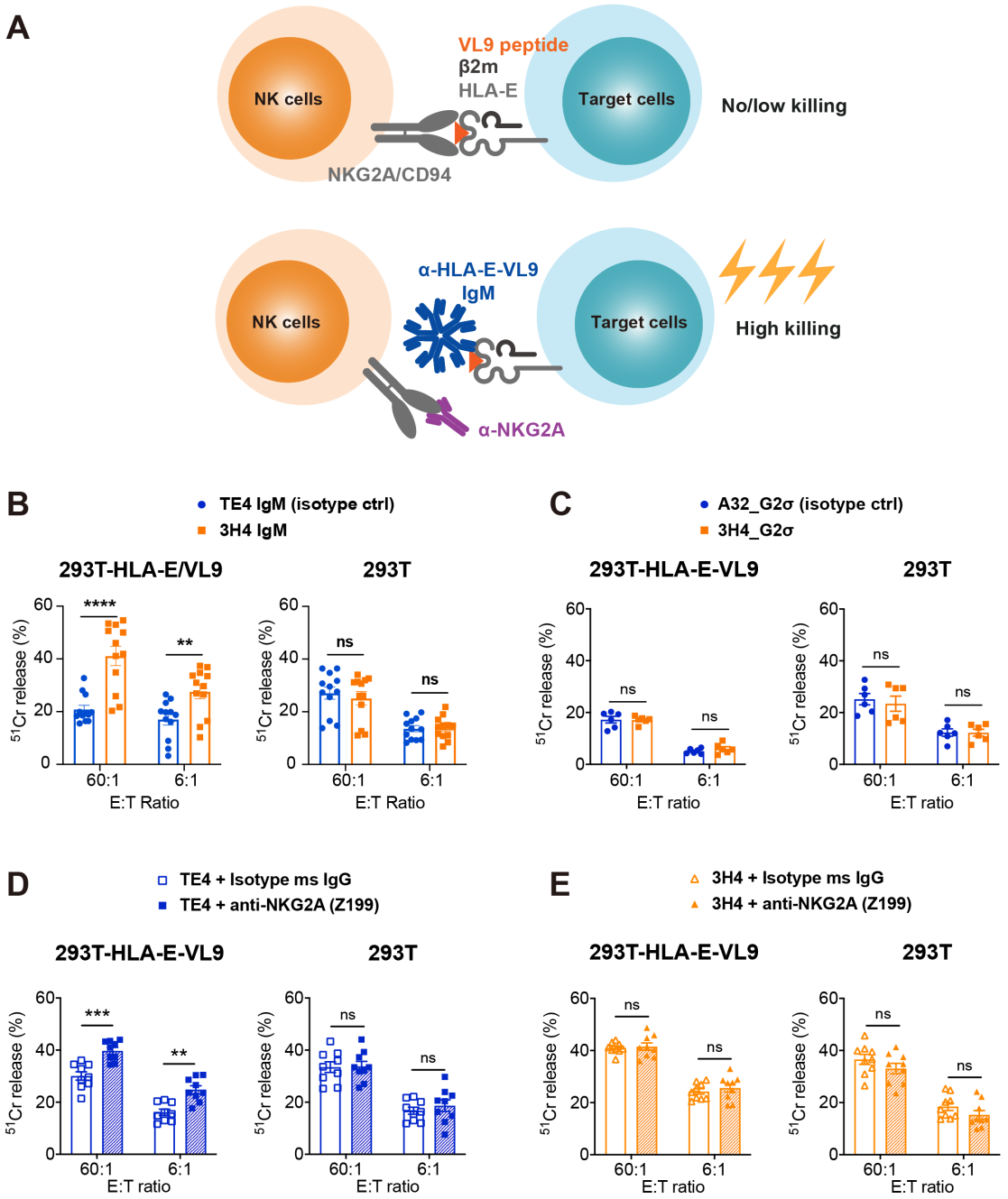

Figure 2. MAb 3H4 enhances cytotoxicity of a NKG2A+ NK cell line against HLA-E-VL9 expressing cells.

(A) Schematic graph of the hypothesis. Blockade of the inhibitory NKG2A/CD94/HLA-E pathway with anti-HLA-E-VL9 antibody (3H4) and/or anti-NKG2A antibody (Z199) could enhance target cell lysis by NK cells.

943 **(B-C) NK cell cytotoxicity against 3H4 IgM (B) or 3H4 IgG (C) treated target cells as**
944 **assessed by ^{51}Cr release assay.** Antibody was incubated with HLA-E-VL9 transfected 293T
945 cells and untransfected 293T cells at final concentration of 10 μg/ml, and NK92 cells were
946 added into the mixture as effector cells. Mouse IgM TE4 or human IgG A32_G2σ were used as
947 isotype controls. Dots represent all the data from four independent experiments, and bars show
948 mean ± SEM.
949 **(D-E) NK cell cytotoxicity in the presence of anti-NKG2A mouse IgG Z199 in combination**
950 **with TE4 control- or 3H4- treated target cells as assessed by ^{51}Cr release assay.** Antibody
951 combinations of Z199 + TE4 control (D) or Z199 + 3H4 (E) were incubated with HLA-E-VL9
952 transfected 293T cells and untransfected 293T cells at a final concentration of 10 μg/ml, and
953 NK92 cells were added into the mixture as effector cells. Dots represent all the data from three
954 independent experiments, and bars show mean ± SEM.
955 The p-values in all the panels were determined by Mann-Whitney U tests. ****, $p<0.0001$; ***,
956 $0.0001<p<0.001$; **, $0.001<p<0.01$; ns, not significant.
957

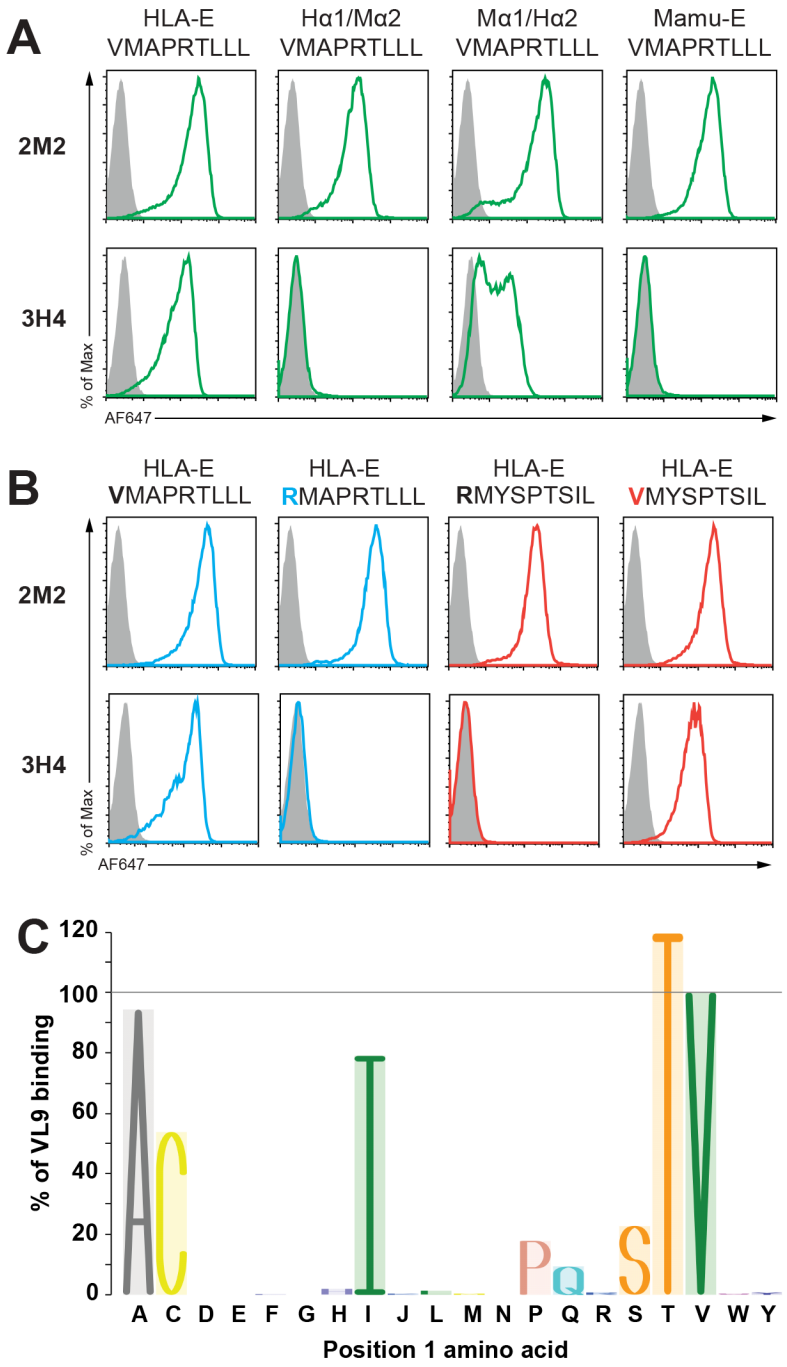

Figure 3. 3H4 recognition of both the HLA-E heavy chain α2 domain and the VL9 peptide. **(A) 3H4 recognizes the α2 domain of HLA-E.** Flow cytometry analysis of 3H4 and 4D12 (HLA-E mAb) binding to 293T cells transfected with VL9 presented by HLA-E, Mamu-E, and two HLA-E/Mamu-E hybrids - one with HLA-E α1/Mamu-E α2 (Hα1/Mα2), the other with Mamu-E α1/HLA-E α2 (Mα1/Hα2) (green). Transfected cells were stained with testing antibody and then

964 an AF647-anti-mouse Ig(H+L) secondary antibody. Isotype control stained cells were used as
965 negative controls (grey filled histograms).
966 **(B) 3H4 recognizes position 1 (P1) of the VL9 peptide.** 3H4 and 2M2 (a control β2M mAb)
967 staining of 293T cells transfected with HLA-E-VL9 (VMAPRTLLL) or HLA-E-VL9 with a mutation
968 at P1 (valine to arginine; RMAPRTLLL) (blue), and with HLA-E-RL9HIV (RMYSPTSIL) or HLA-
969 E-RL9HIV with a mutation at P1 (arginine to valine; VMYSPTSIL) (red). Transfected cells were
970 stained with testing antibody and then an AF647-anti-mouse Ig(H+L) secondary antibody.
971 Isotype control stained cells used as negative controls (grey filled histograms).
972 **(C) 3H4 recognizes peptides with variants in P1**. 293T cells were transfected with HLA-E
973 SCTs with VL9 peptides with single amino acid mutations at P1, then stained with 3H4 antibody
974 followed by AF647 conjugated anti-mouse IgG(H+L) secondary antibody. Cells were gated for
975 EGFP positive subsets. MFI of 3H4 staining on wildtype VL9 peptide was set as 100%, and the
976 percentages equals to (MFI of 3H4 binding on each P1 variant) / (MFI of 3H4 binding on
977 wildtype VL9) x 100%.

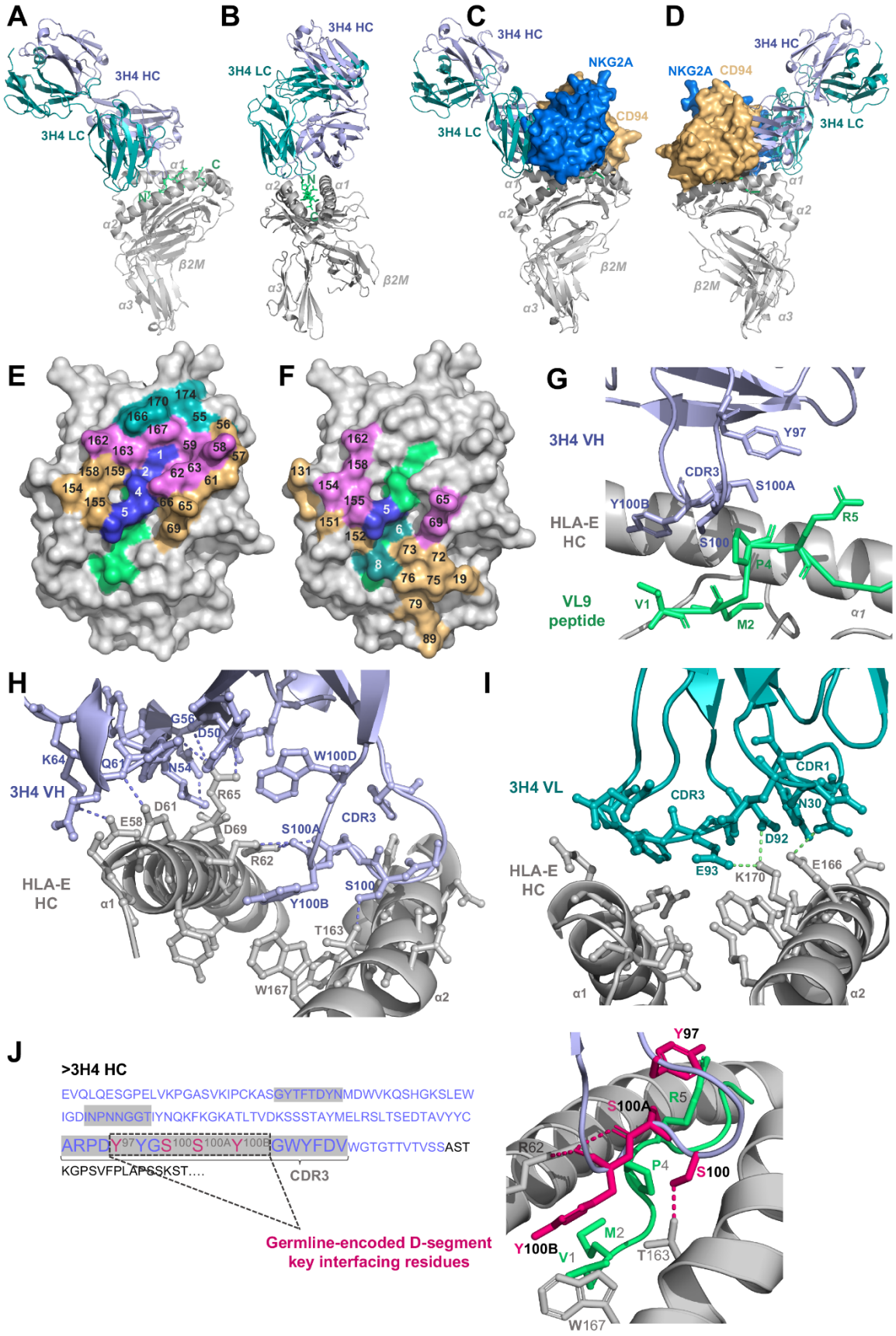
A
3H4 HC
3H4 LC
α1
α2
β2M
α3
B
3H4 HC
3H4 LC
α2
α1
β2M
α3
C
3H4 HC
NKG2A
CD94
3H4 LC
α1
α2
β2M
α3
D
3H4 HC
NKG2A
CD94
3H4 LC
α1
α2
β2M
α3
E
F
G
3H4 VH
Y97
CDR3
S100A
Y100B
HLA-E HC
R5
S100
P4
VL9 peptide
V1
M2
α1
H
3H4 VH
K64
Q61
G56
D50
N54
W100D
R65
D61
E58
D69
S100A
CDR3
R62
HLA-E HC
α1
S100
Y100B
T163
W167
α2
I
3H4 VL
CDR1
CDR3
N30
D92
E93
K170
E166
HLA-E HC
α1
α2
J
>3H4 HC
EVQLQESGPELVKPGASVKIPCKASGYTFTDYNMDWVKQSHGKSLEW
IGDINPNNGGTIYNQKFKGKATLTVDKSSSTAYMELRSLTSEDTAVYYC
ARPDY97YGS100S100AY100BGWYFDVWGTGTTVTVSSAST
KGPSVFPLAPSSKST....
CDR3
Germline-encoded D-segment
key interfacing residues
Y97
S100A
R5
R62
P4
S100
M2
Y100B
V1
T163
W167

978

979 **Figure 4. 3H4 Fab-HLA-E-VL9 co-complex structural visualisation**.

980 **(A-B) 3H4 Fab-HLA-E docking angles.** The HLA-E heavy chain and β2M light chain are shown
981 as a grey cartoon, the VL9 peptide as lime green sticks, the 3H4 HC as a light purple cartoon
982 and the 3H4 light chain (LC) as a teal cartoon.

983 **(C-D) Superposition of 3H4 Fab and CD94/NKG2A docking sites on HLA-E.** The HLA-E
984 complex and 3H4 Fab are color-coded according to A and B. The CD94 subunit is shown as an
985 orange surface and the NKG2A subunit as a marine blue surface.

986 **(E) Aerial view of the HLA-E-VL9 peptide binding groove surface.** Non-interfacing residues
987 of the HLA-E heavy chain are shaded light grey and non-interfacing peptide residues shaded
988 lime green. VL9 peptide residues involved in the 3H4 interface are coloured marine blue.
989 Interfacing HLA-E HC residues that contact the 3H4 VH are shaded orange whereas those that
990 contact the 3H4 VL are shaded teal. HLA-E heavy chain residues involved in the interface with
991 both the 3H4 VH and VL are shaded violet. Residue positions are numbered on the HLA-E
992 surface view.

993 **(F) Aerial view of the overlapping 3H4 and CD94/NKG2A footprints on the HLA-E peptide**
994 **binding groove.** VL9 peptide residues involved in both the 3H4 and CD94/NKG2A interfaces
995 are shaded marine blue whereas HLA-E heavy chain residues involved in both interfaces are
996 shaded violet. Peptide and HLA-E heavy chain residues involved exclusively in the
997 CD94/NKG2A interface are shaded in teal and orange, respectively.

998 **(G) Binding interface of 3H4 HC/VL9 peptide.** Interfacing residues (Y97, S100, S100A and
999 Y100B of the VH CDR3 loop and V1, M2, P4 and R5 of the VL9 peptide) are shown in ball and
1000 stick-form with non-interfacing residues in cartoon form. The VL9 peptide is shaded lime green,
1001 the HLA-E heavy chain in grey and the 3H4 HC in light purple. 3H4 is numbered according to
1002 the Kabat scheme whereby alternate insertion codes (letters after the residue number) are
1003 added to variable length regions of the antibody sequence. Kabat numbering is applied in all
1004 subsequent figures.

1005 **(H-I) Binding interfaces of 3H4 HC/HLA-E heavy chain (H) and 3H4 LC/HLA-E HC (I).**
1006 Interfacing residues are displayed in ball-and-stick form, non-interfacing residues are displayed
1007 in cartoon form and hydrogen bonds as dashed lines. In the 3H4 HC/HLA-E heavy chain
1008 interface (H), interfacing residues derived from the HLA-E heavy chain (grey) include G56, S57,
1009 E58, Y59, D61, R62, E63, R65, S66 and D69 of the α1-helix and E154, H155, A158, Y159,
1010 D162, T163 and W167 of the α2-helix. 3H4 VH (light purple) interfacing residues include N33 of
1011 the CDR1 region, N52, N54, G56 and T57 of the CDR2 region, Y97, G99, S100, S100A, Y100B
1012 and W100D of the CDR3 region and W47, D50, I58, Y59, N60, Q61 and K64 of the non-CDR
1013 VH domain. In the 3H4 LC/HLA-E heavy chain interface (I), HLA-E heavy chain (grey)-derived
1014 interfacing residues include E55, E58, Y59 and R62 of the α1-helix and D162, T163, E166,
1015 W167, K170 and K174 of the α2-helix. 3H4 LC (teal) interfacing residues include Q27, D28, N30
1016 and Y32 of the CDR1 region, D92, E93, F94 and P95 of the CDR3 region in addition to D1 of
1017 the VL domain.
1018 **(J) Key interfacing residues within the germline-encoded D-junction.** 3H4 HC amino acid
1019 sequence with the VH segment in purple and the CDR1/2/3 regions shaded grey. Germline-
1020 encoded residues within the VH CDR3 D-junction are denoted. The 4 key interfacing residues
1021 (Y97, S100, S100A and Y100B) within this germline-encoded D-junction that make contacts
1022 with both the HLA-E heavy chain and VL9 peptide are highlighted magenta in the sequence and
1023 illustrated as magenta sticks in the PyMol visualisation. The HLA-E heavy chain and VL9
1024 peptide are displayed as grey and green cartoons, respectively, with key interfacing residues in
1025 stick form. Hydrogen bonds are depicted as magenta dashed lines and residues of the 3H4 VH
1026 domain that are not germline-encoded key interfacing residues are displayed in light purple
1027 cartoon form.
1028

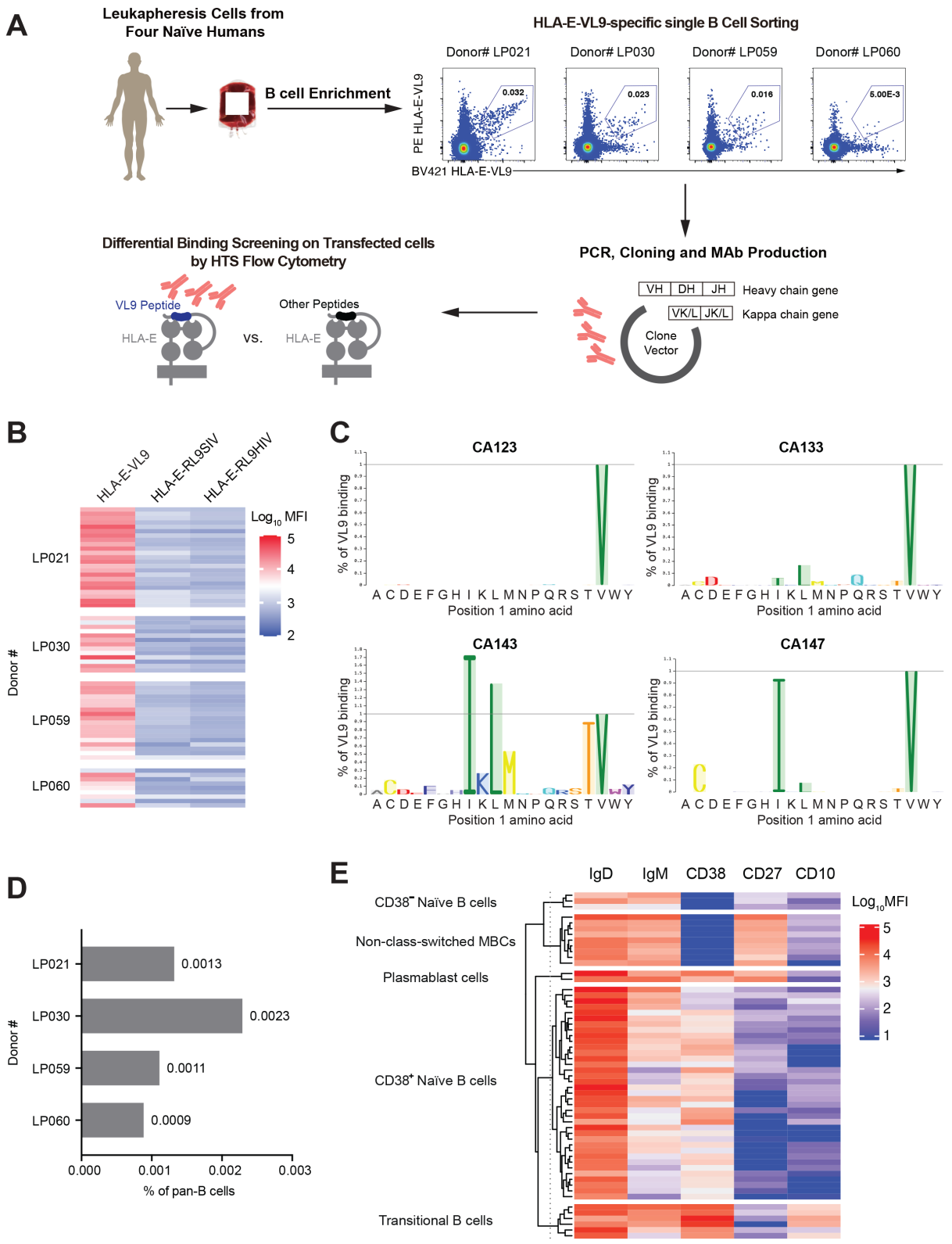

Figure 5. HLA-E-VL9-specific antibodies exist in the B cell pool of healthy humans.

1031 **(A) Scheme of isolating HLA-E-VL9-specific antibodies from healthy humans.** Pan-B cells
1032 were first isolated by negative selection from human leukapheresis PBMCs. A three-color
1033 sorting strategy was used to sort single B cells that were positive for HLA-E-VL9 and negative
1034 for HLA-E-RL9HIV or HLA-E-RL9SIV. Flow cytometry data showing the sorting of HLA-E-VL9
1035 double positive, HLA-E-RL9HIV negative, HLA-E-RL9SIV negative B cells in PBMCs from four
1036 donors (LP021, LP030, LP059 and LP060) are shown. Viable regions of antibody heavy and
1037 light chain genes were isolated from the sorted B cells by PCR, and constructed into an
1038 expression backbone with a human IgG1 constant region. Antibodies were produced by
1039 transient transfection in 293i cells, and antibody binding specificities were analyzed by surface
1040 staining of transfected 293T cells and high throughput screening (HTS) flow cytometry.
1041 **(B) Binding specificities of the HLA-E-VL9-specific antibodies (*n*=56) from four different**
1042 **donors shown as a heatmap.** The compensated MFIs of HLA-E-VL9-specific antibodies
1043 staining on transfected 293T cells at the concentration of 1 μg/ml were shown.
1044 **(C) Mapping of representative HLA-E-VL9-specific mAbs CA123, CA133, CA143 and**
1045 **CA147 on 293T cells transfected with HLA-E-VL9 peptide variants.** 293T cells were
1046 transfected with HLA-E SCTs with VL9 peptides with single amino acid mutations at P1, then
1047 stained with human antibodies CA123, CA133, CA143, and CA147, followed by AF647
1048 conjugated anti-mouse IgG(H+L) secondary antibody (dark blue). Cells were gated for EGFP
1049 positive subsets. MFI of the indicated antibody staining on wildtype VL9 peptide was set as
1050 100%, and the percentages equals to (MFI of binding on each P1 variant) / (MFI of binding on
1051 wildtype VL9) x 100%.
1052 **(D) Percentage of HLA-E-VL9-specific B cells in CD19^{+} pan-B cells in four donors.**
1053 **(E) Phenotypes of HLA-E-VL9-specific B cells (*n*=56) shown as heatmap.** Expression of
1054 markers in each single B cell were determined from index sorting data and are shown as MFIs
1055 after compensation. Compensated MFIs below zero were set as zero. Each row indicates one
1056 single cell. The rows were clustered by K-means Clustering in R. Four subsets were observed:

1057 $CD10^{-}CD27^{-}CD38^{+/-}$ naïve B cells, $CD10^{+}CD27^{-}CD38^{++}$ transitional B cells, $CD10^{-}CD27^{+}CD38^{-}$

1058 non-class-switched memory B cells, and $CD10^{-}CD27^{+}CD38^{+}$ plasmablast cells. Detailed

1059 information for each single cell and antibody is shown in ***Table S6***.

1060

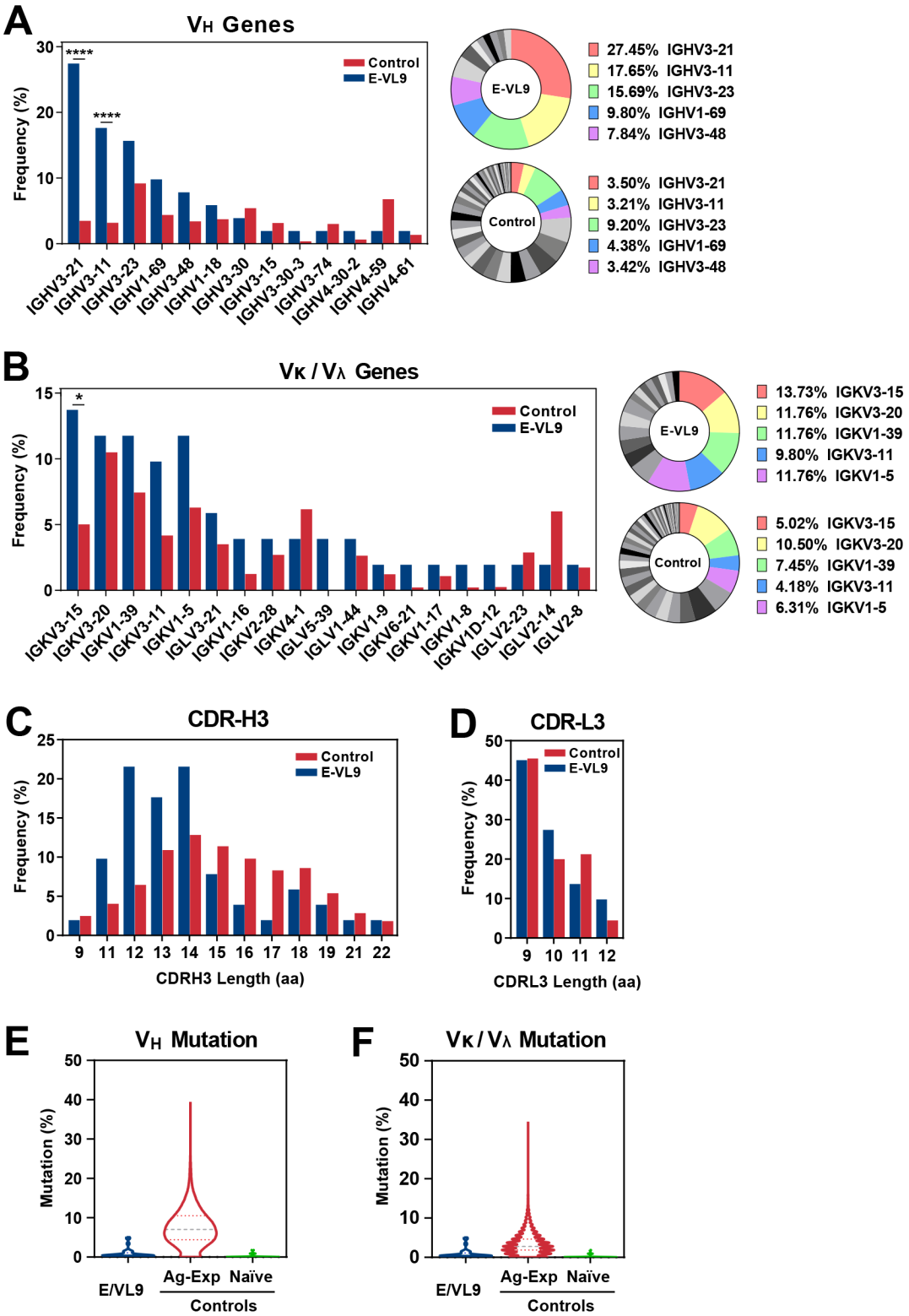

1061

1062 **Figure 6. Sequence analysis of HLA-E-VL9-specific antibodies.** HLA-E-VL9-specific

1063 antibody (n=51) genes isolated from healthy humans were analyzed by Clonalyst and corrected

1064 for clonality. Reference VH-VL repertoires (n=198,148) from three healthy humans from a
1065 previous study (DeKosky et al., 2015) was used as a control for panels A-D Another set of
1066 reference sequences comparing naïve and antigen-experienced (Ag-Exp) antibody repertoires
1067 (n=13,780 and 34,692, respectively) (DeKosky et al., 2016) was used as a control for panel E-F.
1068 The chi-square test of independence was performed to test for an association between
1069 indicated gene usage and repertoire/antibody type in panels A-B. ****, $p<0.0001$; *,
1070 $0.01<p<0.05$.
1071 **(A) Heavy chain viable (V_H) region gene usage shown as a bar chart (left) and pie chart**
1072 **(right).** The top five V_H genes found in HLA-E-VL9-specific antibodies are colored in the pie
1073 charts.
1074 **(B) Kappa chain variable (V_κ) and lambda chain variable (V_λ) region gene usage shown as**
1075 **a bar chart (left) and pie chart (right).** The top five V_κ/V_λ genes found in HLA-E-VL9-specific
1076 antibodies are colored in the pie charts.
1077 **(C) Comparison of heavy chain CDR3 (CDR-H3) length.**
1078 **(D) Comparison of light chain CDR3 (CDR-L3) length.**
1079 **(E-F) Violin plots showing the mutation rates of heavy chains (H) and light chains (I).**
1080
1081

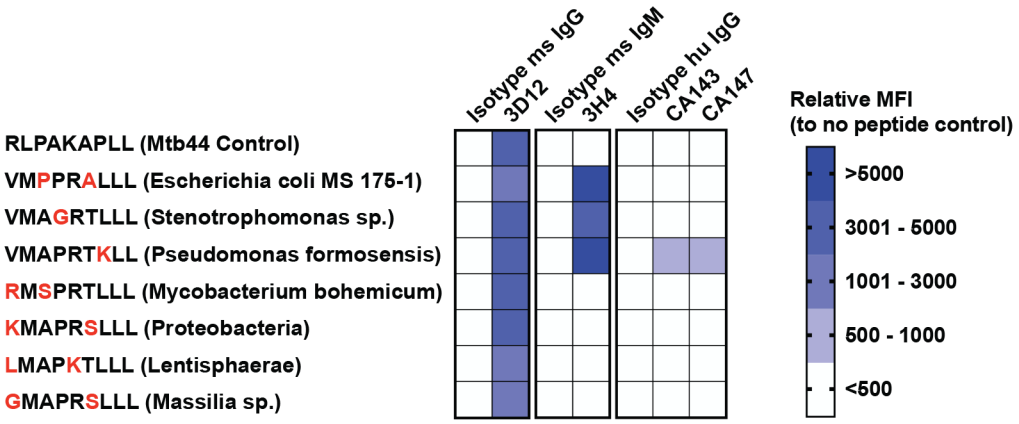

Figure 7. HLA-E-VL9-specific antibodies cross-react with certain microbiome-derived peptides presented by HLA-E. K562 cells loaded with microbiome-derived peptides were stained with the indicated antibodies at a concentration of 10 μg/ml. Binding activities are shown in heatmap form with relative MFIs (MFI of peptide-loaded cells minus MFI of no peptide control cells) depicted on the scale shown.